FLUID MODELING OF EXHAUST GAS DISPERSION FROM THE PARCEL 7 VENTILATION SITE, CENTRAL ARTERY/THIRD HARBOR TUNNEL PROJECT

Prepared by

David E. Neff
Thomas Z. Tan
Robert N. Meroney

Final Report
(June 1988 - December 1988)

for

Bechtel/Parsons Brinkerhoff
Central Artery/Third Harbor Tunnel Project
One South Boston
Boston, Mass. 02110

FLUID MECHANICS AND WIND ENGINEERING PROGRAM

Colorado State University

CSU Contract No. 2-97360
CER88-89DEN-TZT-RNM-6

FLUID MODELING OF EXHAUST GAS DISPERSION FROM THE PARCEL 7 VENTILATION SITE, CENTRAL ARTERY/THIRD HARBOR TUNNEL PROJECT

FINAL REPORT

(July 1988 - December 1988)

Prepared by

David E. Neff*
Thomas Z. Tan*
Robert N. Meroney+

Fluid Mechanics and Wind Engineering Program
Civil Engineering Department
College of Engineering
COLORADO STATE UNIVERSITY
Fort Collins, Colorado 80523

for

Bechtel/Parsons Brinkerhoff
Central Artery/Third Harbor Tunnel Project
One South Boston
Boston, Mass. 02110

CSU Contract No. 2-97360

* Research Associate
\+ Professor, Civil Engineering

CER88-89DEN-TZT-RNM-6

Colorado State University

EXECUTIVE SUMMARY

Title: Fluid Modeling of Exhaust Gas Dispersion from the Parcel 7 Ventilation Site, Central Artery/Third Harbor Tunnel Project

Contractors: Civil Engineering Department
Colorado State University
Fort Collins, Colorado 80523

Principal Investigators: D.E. Neff, T.Z. Tan and R.N. Meroney

Report Period: July 1988 - December 1988

Objective: The Commonwealth of Massachusetts, in cooperation with the Department of Transportation, Federal Highway Administration, proposes to depress and widen the Central Artery through central Boston. The underground sections of the Central Artery and the Third Harbor Tunnel will be ventilated. Seven ventilation buildings are planned for the project. Two of the building sites, Parcel 7 and Boston Edison, are located in congested, heavily populated areas within the confines of downtown Boston. The complicated flow patterns associated with these sites clearly indicate the need for physical modeling of vent building air quality impacts. The Fluid Dynamics and Diffusion Laboratory at Colorado State University has conducted the wind tunnel physical modeling study requested by B/PB. The objectives of this model study were a) to provide visual information and concentration data on the environmental impact of several proposed vent building configurations, stack height specifications, and b) summarize this information and data into a convenient format then discuss the advantages and disadvantages of the different vent building-stack specifications.

Results: Selection of the final building and exhaust stack configuration for the Parcel 7 Ventilator building will be based upon the consideration of its visual appearance within the Boston historic district, zoning regulations, and minimization of environmental impact. The environmental effects of exhaust from the ventilator stacks will depend upon tunnel traffic volume, ventilator flow rates, state and federal ambient air-quality regulations, building and plume aerodynamics, and local meteorology. This study evaluates through fluid modeling the influence of building and plume aerodynamics on plume dilution. Data is reported in terms of normalized concentrations (K coefficients) to

permit concentration estimates for alternative traffic, exhaust and wind speed conditions. Concentrations can be estimated for alternative configurations, but acceptability must depend upon current air-quality standards.

TABLE OF CONTENTS

LIST OF TABLES

LIST OF FIGURES

LIST OF SYMBOLS

A,B,C	Constants
BR	Blockage ratio
C_p	Specific heat capacity at constant pressure
E	Hot wire voltage output
h	Height of the obstacle
g	Gravitational acceleration
k	Roughness length
L	Length
Q	Flow rate
S	Distance downstream of the obstacle
T	Temperature
U	Wind velocity
u_*	Friction velocity
W	Stack velocity
X	Concentration
x	Distance
Z	Height above ground
z_o	Roughness length

Greek Characters

ρ	Air density
Γ	Adiabatic potential temperature lapse rate
κ	Thermal conductivity
μ	Dynamic viscosity
ν	Kinematic viscosity
ρ	Density
χ	Fraction of a gas component
Ω	Angular velocity of earth - $0.726*10^{-4}$ rad/s

Dimensionless Parameters

Ec	Eckert number
Ma	Mach number
Re	Reynolds number
Ri	Bulk Richardson number
Ro	Rossby number
Pr	Prandtl number
V	Volume flux ratio ($Q/U_H L^2$)

1. INTRODUCTION

The Commonwealth of Massachusetts, in cooperation with the Department of Transportation, Federal Highway Administration, proposes to depress and widen the Central Artery through central Boston. The Bechtel/Parsons Brinkerhoff (B/PB) joint venture has been selected by the Commonwealth of Massachusetts to manage the Central Artery and Third Harbor Tunnel Project. The work performed by B/PB is under the direction of the Massachusetts Department of Public Works (MADPW).

The underground sections of the Central Artery and the Third Harbor Tunnel will be ventilated. Seven ventilation buildings are planned for the project. Two of the building sites, Parcel 7 and Boston Edison, are located in congested, heavily populated areas within the confines of downtown Boston. The complicated flow patterns associated with these sites clearly indicate the need for physical modeling of vent building air quality impacts.

The Fluid Dynamics and Diffusion Laboratory at Colorado State University has conducted the wind tunnel physical modeling study requested by B/PB. The objectives of this model study are:

1. To provide visual information and concentration data on the environmental impact of several proposed vent building, stack height specifications, and
2. Summarize this information and data into a convenient format then discuss the advantages and disadvantages of the different vent building-stack specifications.

These objectives will be separately carried out for a Phase 1 series of tests oriented on the Parcel 7 building region and a Phase 2 series of tests oriented on the Boston Edison building region. This report deals only with the Phase 1 study.

Section 2.0 discusses the physics of modeling plumes at reduced length scales. Section 3.0 describes the data acquisition techniques used to perform this study. Section 4.0 lists the test program results. Section 5.0 is a discussion of selected data.

2. MODELING OF PLUME DISPERSION FROM TUNNEL VENTILATOR SITES

The Appendix describes in general terms the scaling laws that cover a large class of fluid modeling applications. The intent of this section is to specifically address the modeling techniques used in the present study.

The exhaust air released from the tunnel ventilators will exit at ambient temperatures and densities; hence, the source gas used in the model was primarily nitrogen released at room temperatures (specific gravity ≈ 1.0). Thus the plume mass flux, momentum flux and volume flux are essentially equivalent ratios, and the plume Froude number is not a relevant parameter.

The wind approaches the Boston city center over either suburban roughness or the harbor sea surface. The Parcel 7 site is located within the central portion of downtown Boston surrounded by large buildings. Replicas (at reduced scale of 1:384) of all buildings within 2,300 feet of the Parcel 7 vent building were constructed and placed on the downwind turntable in the wind tunnel. The approach flow characteristics approaching the Parcel 7 site and surroundings were simulated with a generic suburban roughness constructed from one-inch cubes.

The modeling parameter decision process yielded the following conclusions:

1. Maximum field dispersion distance of interest and size of the FDDL Environmental Wind Tunnel facility resulted in the selection of a 1:384 model length scale ratio.

2. Neutral stratification in the laboratory was used to reproduce the dispersion dynamics of the windy Boston area.

3. Wind-tunnel floor roughness was adjusted to produce properly scaled wind shear and turbulent structure.

4. Model wind speed and stack exit velocity were set at large enough magnitudes to assure Reynolds number independence of approach flow and stack flow.

5. Model wind velocity to plume velocity ratios were set equal to the field values; thus assuring similarity of plume trajectories.

3. DATA ACQUISITION AND ANALYSIS TECHNIQUES

Laboratory measurement techniques are discussed in this section, along with conversion methods used to convert measured model quantities to their meaningful field equivalents. Some of the methods used are conventional and need little elaboration.

3.1. WIND-TUNNEL FACILITIES

The experiments were performed in the Environmental Wind Tunnel (EWT) shown in Figure 1. This wind tunnel, especially designed to study atmospheric flow phenomena, incorporates special features such as an adjustable ceiling, a rotating turntable and a long test section to permit adequate reproduction of micrometeorological behavior. Mean wind speeds of 0.1 to 15 m/sec in the EWT can be obtained. Boundary-layer thickness up to 1.2 m can be developed "naturally" over the downstream 6 m of the EWT test section by using vortex generators at the test section entrance and surface roughness on the floor. The flexible test section on the EWT roof is adjustable in height to permit the longitudinal pressure gradient to be set at zero.

3.2. WIND PROFILE MEASUREMENTS

Velocity measurements were made with single-hot-film probes and anemometry equipment manufactured by Thermo-System, Inc. (TSI).

Velocity Standard

The velocity standard used in the present study consisted of a Matheson Model 8116-0154 mass flowmeter and a profile conditioning section designed and calibrated by the Fluid Dynamics and Diffusion (FDDL) staff at Colorado State University (CSU). The mass flowmeter measures mass flow rate independent of temperature and pressure. The profile conditioning section forms a flat velocity profile of very low turbulence at the position where the hot-film-probe is located. Incorporating a measurement of the ambient atmospheric pressure, temperature and a profile correction factor permits the calibration of velocity at the measurement station from 0.15-2.2 m/s to within ± 5 percent.

Single-Hot-Film Probe Measurements

Single-hot-film (TSI 1210 Sensor) measurements were used to document the longitudinal turbulence levels for the approach flow conditions. During calibration the probe voltages were recorded at several velocities covering the range of interest. These voltage-velocity (E,U) pairs were then regressed to the equation $E^2 = A + BU^c$ via a least squares approach for various assumed values of the exponent c. Convergence to the minimum residual error was accelerated by using the secant method to find the best new estimate for the exponent c.

The hot-film-probe was mounted on a vertical traverse and positioned over the measurement location in the wind tunnel. The anemometer's output voltage was digitized and stored within an IBM AT computer. This voltage time series was converted to a velocity time series using the inverse of

the calibration equation; $U = [(E^2 - A)/B]^{1/c}$. The velocity time series was then analyzed for pertinent statistical quantities, such as mean velocity and root-mean-square turbulent velocity fluctuations. The computer system would move the velocity probe to a vertical position, acquire the data, then move on to the next vertical positions, thus obtaining an entire vertical velocity profile automatically.

Error Statement

The calibration curve yielded hot film anemometer velocities that were always within 2 percent of the known calibrator velocity. Considering the accumulative effect of calibrator, calibration curve fit and other errors the model velocity time series should be accurate to within 10 percent.

3.3. FLOW VISUALIZATION TECHNIQUES

A visible plume was produced by passing the metered simulant gas through a smoke generator (Fog/Smoke Machine manufactured by Roscolab, Ltd.) and then out of the modeled stack. The visible plumes for each test were recorded on VHS video cassettes with a Panasonic Omnivision II camera/recorder system. Run number titles were placed on the video cassette with a title generator.

3.4. CONCENTRATION MEASUREMENTS

The experimental measurements of concentration were performed using a Hewlett Packard gas-chromatograph and sampling systems designed by Fluid Dynamics and Diffusion Laboratory staff.

3.4.1. *Gas Chromatograph*

A gas chromatograph (Hewlett-Packard Model 5710A) (GC) with flame ionization detector (FID) operates on the principle that the electrical conductivity of a gas is directly proportional to the concentration of charged particles within the gas. The ions in this case are formed by the burning a mixture of hydrogen and the sample gas in the FID. The ions and electrons formed pass between an electrode gap and decrease the gap resistance. The resulting voltage drop is amplified by an electrometer and passed to a Hewlett-Packard Model 3390A integrator. When no effluent gas is flowing, a carrier gas (nitrogen) flows through the FID. Due to certain impurities in the carrier, some ions and electrons are formed creating a background voltage or zero shift. When the effluent gas enters the FID, the voltage increase above this zero shift is proportional to the degree of ionization or correspondingly the amount of tracer gas present. Since the chromatograph used in this study features a temperature control on the flame and electrometer, there is very low drift of the zero shift. Even given any zero drift, the HP 3390A, which integrates the effluent peak, also subtracts out the zero drift.

The lower limit of measurement is imposed by the instrument sensitivity and the background concentration of tracer within the air in

the wind tunnel. Background concentrations were measured and subtracted from all data quoted herein.

3.4.2. *Sampling System*

The tracer gas sampling system consists of a series of fifty 30 cc syringes mounted between two circular aluminum plates. A variable-speed motor raises a third plate, which lifts the plunger on all 50 syringes, simultaneously. Computer controlled valves and tubing are connected such that airflow from each tunnel sampling point passes over the top of each designated syringe. When the syringe plunger is raised, a sample from the tunnel is drawn into the syringe container. The sampling procedure consists of flushing (taking and expending a sample) the syringe three times after which the test sample is taken. The draw rate is variable and generally set to be approximately 6 cc/min.

The sampling system was periodically calibrated to insure proper function of each of the valves and tubing assemblies. To calibrate the sampler each intake was connected to a manifold. The manifold, in turn, was connected to a gas cylinder having a known concentration of tracer gas. The gas was turned on, and a valve on the manifold was opened to release the pressure produced in the manifold. The manifold was allowed to flush for about one minute. Normal sampling procedures were carried out during calibration to insure exactly the same procedure is reproduced as when taking a sample from the tunnel. Each sample was then analyzed for tracer gas concentration. Percent error was calculated, and "bad" syringe/tube systems (error > 2 percent) were not used or repaired.

3.4.3. *Test Procedure*

The test procedure consisted of:

1) Setting the proper tunnel wind speed,
2) Releasing the metered mixtures of source gas from the plant stack,
3) Withdrawing samples of air from the tunnel designated locations, and
4) Analyzing the samples with a FID.

The samples were drawn into each syringe over a 200 s (approximate) time period and then consecutively injected into the GC.

The procedure for analyzing the samples from the tunnel is:

1) Introduce the sample into the GC which separates the ethane tracer gas from other hydrocarbons,
2) The voltage output from the chromatograph FID electrometer is sent to the HP 3390A Integrator,
3) the HP 3390A communicates the measured concentration in ppm to an IBM computer for storage, and

4) These values, χ_{mea}, along with the response levels for the background χ_{bg} and source χ_{source} are converted into source normalized model concentration by the equation:

$$\chi_m = \frac{\chi_{mea} - \chi_{bg}}{\chi_{source} - \chi_{bg}}$$

5) Field equivalent concentration values are related to model values by the equation:

$$\chi_p = \frac{\chi_m}{\chi_m + (1-\chi_m)[(\frac{T_a}{T_s})V]_m/[(\frac{T_a}{T_s})V]_p}, \quad \text{where } V = Q/U_H L^2,$$

and L is a characteristic length scale. When there is no distortion in the model-field volume flux ratio, V, and the plumes are isothermal this equation reduces to $\chi_p = \chi_m$.

Error Statement

Finite background concentrations, χ_{bg}, resulted from previous tests within the laboratory, these low levels could be measured to accuracies of 20 percent. The larger measured concentrations, χ_{mea}, were accurate to 2 percent. The source gas concentration, χ_{source}, was known to within 10 percent. Thus the source normalized concentration for $\chi_{mea} >> \chi_{bg}$ was accurate to approximately 10 percent. For low concentration values, $\chi_{mea} > \chi_{bg}$, the errors are larger.

4. TEST PROGRAM AND DATA FOR PARCEL 7 (PHASE 1)

A physical modeling study of the Parcel 7 vent building was performed to assist in predicting environmental impacts for several proposed stack-building configurations. This involved:

1) The 1:384 reduced scale construction of the different potential Parcel 7 stack-building configurations along with the all buildings within 2300 feet of the Parcel 7 site,
2) The placement of this model into a wind tunnel facility with the appropriate upwind roughness for this site,
3) Acquisition of velocity and turbulence profiles approaching and at the modeled Parcel 7 site for each wind direction of interest,
4) Video taping of the model plume for 197 different combinations of stack-building height and type, wind direction and stack exit velocities,
5) Concentration measurements at 49 different sampling locations for 67 different combinations of stack-building height and type, wind direction and stack exit velocities, and
6) The presentation of a final report that lists all data and discusses all experimental techniques used to acquire this data.

The following sub-sections discuss these topics in greater detail.

4.1. MODEL CONSTRUCTION

Based on atmospheric data over the Boston area, the size of the concentration grid, and modeling constraints discussed in Section 2 and the Appendix, a model scale of 1:384 was selected. Since the Environmental Wind Tunnel (see Figure 1) had a 12 foot turntable this allowed for the reduced scale construction of all significant buildings within a 2300 foot radius of the Parcel 7 vent building site. The location of the Parcel 7 site along with a circle demarking the portion of downtown Boston which was replicated is shown in Figure 2.

The buildings surrounding the vent structure were fabricated from styrofoam and were placed in their appropriate locations on a 12 foot diameter 1/4 inch masonite sheet. All roads and waterways were painted on this masonite sheet. The topography changes were modeled by layering several 1/4 inch sheet to match the land contours within the modeled area. Figure 3 is a picture looking upwind of the entire 12 foot turntable model located inside the wind tunnel. Note in this picture that the terrain upwind of the turntable area was modeled with a generic roughness with a field equivalent height of 32 feet (1 inch cubes).

The Parcel 7 vent building was built in a modular form so that an array of different building, garage and stack heights could be tested. The different building heights possible were 53, 75, 90 and 375 feet. The garage heights varied from 42, 75 and 90 feet. The stack heights were 100, 115, 125, 150, 225 and 400 feet. Figure 4 through Figure 8 show pictures of some of the common configurations of building-garage-stack heights tested. The different building and garage modules were

constructed of masonite, whereas the stacks were fabricated from tack board. The smallest building module contained a manifold through which metered simulate gases were directed to the stacks. The Parcel 7 ventilator building used 14 vent fans to blow exhaust gases through 10 by 14 foot (inside measure) openings. These individual stacks were arranged into 2 groups of 4 openings and 2 groups of 3 openings. The spacing between these 4 stack groups could also be varied. The intake ports for the Parcel 7 complex were modeled by connecting a metered vacuum source to the inlet portion of the building that was constructed of screen.

Plume dispersion from a proposed Charles river vent site was also studied with this same Boston model. This vent building location is depicted in Figure 2 out on the edge of the modeled area. The Charles river vent building was 100 feet tall and the stack were 200 feet high. Figure 9 shows a picture of the modeled structure. This vent site used 6 fans to blow exhaust gases through 10 by 14 foot openings. These stacks were organized into 3 groups of 2 openings each.

4.2. VELOCITY PROFILES

The techniques employed in the acquisition of velocity profiles are discussed in Section 3.2. An approach flow upwind of the turntable model, typical of a suburban environment, was created through the placement of vortex generators at the tunnel entrance followed by 30 feet of 1 inch cube roughness on the tunnel floor. The site model was located on a turntable, thus it could be rotated to simulate the different wind directions.

Table 1 summarizes the conditions for all the velocity profiles obtained in this study. Table 2 through Table 5 present the data for each of these profiles. Figure 10 through Figure 17 display plots of these mean velocity and longitudinal turbulent intensity profiles. The height coordinate in these tables and figures has been normalized by a model reference height of 1 meter (equivalent field height of 1260 feet); thus, to obtain actual field heights multiply the normalized value by 1260. The velocity coordinate in these tables and figures has been normalized by the model velocity at 1 meter height. The model reference velocities used for each of the profiles are listed in Table 1. Since a neutral boundary layer's velocity is invariant with respect to wind speed the normalized profiles presented can be converted to any field velocity at a specific height by the appropriate multiplicative constant.

The first three profiles (numbers 1, 2 and 3) tested the crosswind uniformity of the flow approaching the modeled site. The data for these profiles are tabulated in Table 2. The mean velocity profiles are shown in Figure 10 and the turbulent intensity profiles are shown in Figure 11. These figures and table show that the wind tunnel crosswind uniformity was good.

The next three profiles (numbers 4, 5 and 6) tested the invariance of the mean and turbulent velocity profiles with respect to different wind tunnel reference wind speeds. The data for these profiles are tabulated

in Table 3. The mean velocity profiles are shown in Figure 12 and the turbulent intensity profiles are shown in Figure 13. These figures and table show that the wind tunnel approach flow was indeed invariant with respect to wind speed.

The approach mean velocity profiles (numbers 1 to 6) were regressed to find the best log-log and log-linear fit. The log-log regression produced a power law exponent, p, equal to 0.24; i.e. $U/U_r = (z/z_r)^p$. The log-linear regression ($U/u_* = 2.5\ln\{(z-d)/z_o\}$) found a best fit roughness length, z_o, of 0.9 meters (field scale) and a displacement thickness, d, of 4.8 meters. These values of the power law exponent and the roughness length are appropriate for a suburban roughness condition.

The next eight profiles (numbers 7 through 14) were obtained over the center of the model at the Parcel 7 ventilator site. Each profile was for a primary wind directions from 0° to 360° at 45° increments. The wind direction for each of these profiles is listed in Table 1. The profile data for wind directions 0° through 135° are tabulated in Table 4. The mean velocity profiles are shown in Figure 14 and the turbulent intensity profiles are shown in Figure 15. The profile data for wind directions 180° through 315° are tabulated in Table 5. The mean velocity profiles are shown in Figure 16 and the turbulent intensity profiles are shown in Figure 17. These two sets of figures show the influence of upwind structures on the local velocities over the Parcel 7 site. The most radical influence of upwind structures on the wind is seen in profile number 12 where the wind direction was 225° (SW) from the north.

4.3. VISUALIZATION TEST RESULTS

Techniques employed to obtain a visible plume are discussed in Section 3.3. Table 6 show the test conditions for 197 flow visualization tests over the Parcel 7 building region. Three different stack exhaust flow rates were considered for a variety of wind directions and various building configurations. Two ventilation building sites were evaluated, i.e. one at the Parcel 7 location and one at the Charles river location. The field equivalent wind velocity for all these tests was 5 m/s at 30 meters height approaching the modeled area. The model velocity was 0.5 m/s at 0.078 meter height (0.078 m = 30/384) approaching the model area. This wind speed was chosen to maintain flow similarity between the wind tunnel and the actual conditions. The field wind velocity at other heights above the Parcel 7 site for a specific wind direction may be calculated by the following procedure:

1) The approach flow velocity profiles taken just upwind of the turntable model area indicate that when a 5 m/s (16.4 ft/s) velocity exists at a 30 meter height then the velocity at 384 meters is 5*(1/0.552) = 9.05 m/s (the normalized velocity on profiles 1 to 6 at height 0.078 is roughly 0.552), and

2) Multiplying the normalized velocity values in the profile of interest (see section 4.2 above) by 9.05 m/s (29.7 ft/s) will yield the velocity at the desired height.

Figure 18 and Figure 19 display pictures of two different visual plume tests.

Table 10 lists for each of the 197 visual test runs observations on stack downwash, building downwash, cavity mixing, plume descent, plume lofting, skyscraper impingement and other pertinent comments. Documentation on video cassettes of all visual tests have been provided to the sponsor prior to this report. Given a field to model wind speed ratio of 10 (= [5 m/s]/[0.5 m/s]) and a model to field length scale ratio of 384, then the time scale ratio between the model and the field is 1:38.4. Thus phenomena observed over the model in the wind tunnel will occur 38.4 times faster than observed at full scale. If the TV tapes were replayed in slow motion (38.4 times slower than the recorded speed), the observed plume trajectories and motions would appear realistic.

4.4. CONCENTRATION DATA RESULTS

By maintaining flow similarity between model and field conditions, relative concentrations (χ/Q) for a given source configuration, building configuration and wind direction will be invariant. The wind tunnel relative concentration measurements for the Parcel 7 vent building will be the same as those that could be obtained during full-scale measurements under the same ambient conditions. Since the initial plume path depends upon the ratio of exhaust velocity, W , to wind speed, U, the distribution of the relative concentration field will change for different values of W/U.

From the smoke visualization tests it was determined that varying the vent stack grouping produced very little noticeable differences in plume trajectories. Varying the garage building heights produced a similar effect to varying the building height. The WSW and SE wind directions were identified as critical directions having the potential for high concentrations. Hence concentration measurements were performed over a test matrix of 67 conditions to evaluate the quantitative influence of those parameters which did appear to influence concentrations--stack height, stack velocity, and building orientation.

Techniques employed to obtain the concentration data are discussed in Section 3.4. Table 13 describes the 49 sampling locations and provides the associated building code number, building description and distances from model center. The model distances are the actual measured values on the model turntable, and while the prototype values are the values extrapolated based on the scale ratio. Figure 20 shows all the concentration sampling locations marked on a map of the modeled area. Figure 21 shows a schematic of the manner simulant stack gases were introduced into the wind tunnel and subsequently sampled for concentration analysis. Table 14 summarizes the concentration test conditions for all 67 runs performed. The field and model wind speeds indicated in this table were at 30 meters and 7.9 cm, respectively. The conversion from these upwind velocity values to local values above the Parcel 7 site is the same as that described previously in Section 4.3 above.

Table 15, Table 16, Table 17, Table 18, Table 19 present the normalized concentration data, $(\chi U_H/Q)*10^9$, for all tests. This normalized concentration has units of ft^{-2}. This normalized format is convenient because the concentration results, χ, from a test at one particular combination of wind speed, U_H, and flow rate, Q, can be extrapolated to other U_H, Q values provided that the ratio, U_H/Q, remains the same. Note that U_H is the wind speed at 30 meters height approaching the model area and not the value of wind speed above the vent site. The total flow rate, Q, out of the stacks is the exit velocity for a particular run times the total stack exit area. The stack exit velocities for each run are listed in Table 14. The total exit area for the Parcel 7 vent stacks was always 1960 ft^2. The total exit area for the Charles river site was always 840 ft^2

5. DISCUSSION AND RECOMMENDATIONS

Selection of the final building and exhaust stack configuration for the Parcel 7 Ventilator building will be based upon the consideration of its visual appearance within the Boston historic district, zoning regulations, and minimization of environmental impact. The environmental effects of exhaust from the ventilator stacks will depend upon tunnel traffic volume, ventilator flow rates, state and federal ambient air-quality regulations, building and plume aerodynamics, and local meteorology. This study evaluates through fluid modeling the influence of building and plume aerodynamics on plume dilution. Data is reported in terms of normalized concentrations K,

$$K = \chi U/Q,$$

to permit concentration estimates for alternative traffic, exhaust and wind speed conditions. Concentrations can be estimated for alternative configurations, but acceptability must depend upon current air-quality standards.

The following discussion will first consider implications of the visualization tests. Next it will focus upon evidence for reliability and consistency within the concentration data set, and ,finally, comments will be made on the advantages or disadvantages of different building and stack configurations.

5.1. SMOKE VISUALIZATION RESULTS

As noted in Section 4.3 a total of 197 smoke test cases were performed to evaluate the relative dispersion that occurs for various vent stack heights, vent stack groupings, exit flow velocities, vent building configurations and site orientations. Tests were grouped to examine the relative effects of stack height, exit flow velocity, vent stack grouping, vent building height, adjacent garage height, and site orientation. Table 10 to Table 12 summarize observations of plume behavior for each visualization run. The observations note the presence or absence of

i)	Stack downwash	-	plume flagging or suction of smoke into stack wake
ii)	Building downwash	-	suction of plume downward into building cavity
iii)	Cavity mixing	-	mixing of plume throughout downwind building cavity
iv)	Plume descent	-	deflection of plume groundward over building cavity
v)	Plume lofting	-	plume little influenced by building, plume remains aloft
vi)	Skyscraper impingement	-	Elevated plume stagnates against faces of downwind tall buildings

The cases studied may be categorized and grouped to reveal data trends. Examination of the visual records of these experiments reveals:

a) Stack Height (ft): 100, 125, 150, 225 and 400.

Examination of runs with equivalent building and garage heights as well as constant exhaust velocities reveals the relative value of increased stack height. A 100 foot stack permits significant building downwash, whereas the building geometry does not appear to perturb the plume for stacks greater than 150 feet. Plumes released at heights greater than 150 feet loft above the building cavity and enter the building wake after it has merged with perturbations produced by other obstructions. For some situations with a 100 foot stack the plume was brought to the ground in the street directly downwind of the Parcel 7 building.

b) Exit Flow Velocity (ft/min): 800, 1600, 3200.

The vent gases are expected to exhaust at near ambient temperatures; hence, the vent plume will have little or no thermal buoyancy. Thus, plume rise will occur only as a result of vertical momentum. Higher exit flow velocities will add effective height to the vent stack. In addition low exhaust velocities ($W/U < 1.5$) may permit local downwash behind the vent stack, reducing the effective stack height significantly. Tests show that the 800 ft/min exhaust velocity permits severe downwash of the plume down the side of the stack directly into the building cavity. A 1600 ft/min exhaust velocity in a 5 m/sec wind field ($W/U = 1.6$) minimizes local stack downwash effects. Exhaust velocities greater than 1600 ft/min increase the effective plume release height, but the apparent reduction in plume/building interaction is small once stack downwash is eliminated.

c) Vent Stack Grouping: i) separate stack for each zone
ii) zones 1 & 2 combined.
zones 3 & 4 combined.

Several tests were performed to determine if different roof top arrangements of the vent stacks might reduce downwash effects. The conditions varied from separate stacks to a case with all vents combined. Unfortunately, the roof area was not great enough to permit significant separation; hence, no significant differences were observed.

d) Vent Building Height (ft): 53, 75, 90, and 375.

Several vent building heights were examined to determine if an optimum building height could be identified. For a constant stack height downwash was greater as the building height to stack height ratio decreased. On the other hand apparent dilution of the smoke also occurred as the smoke mixed over greater building

cavity volumes. When tall buildings were combined with tall stacks the exhaust gases often lofted over the immediate neighborhood entirely, since the effective stack height now exceeded 2.5 times the minimum building dimension. If the 90 and 375 foot building heights are judged to be unacceptable, a 75 foot building would produce acceptable plume trajectories when combined with stack heights equal to or greater than 125 feet.

e) Adjacent Connected Garage Height (ft): 42, 75, 90, 375.

Various garage building heights were combined with the different Parcel 7 building heights. They were analyzed to evaluate their combined influence on the vent plume. At no time was the combined building height greater than the Parcel 7 building height; hence, the general shape of the building wake cavity was only slightly perturbed. The results were similar to those of the building height tests with minimum garage heights with only small changes in plume trajectory or dilution.

f) Site Orientation: N, NNE, NE, ENE, E, ESE, SE, SSE, S, SSW, SW, WSW, W, WNW, NW, NNW.

The model was rotated to allow approach winds from the 16 major compass points. As the flow interacted with upwind buildings and the shape of the Parcel 7 building the vent plume trajectory was modified by the variation in streamline patterns.

Several patterns reoccurred no matter the building configuration examined. Winds over the Boston financial district from the W through NW directions were blocked by the tall buildings, which produced a sheltered low-wind region at the Parcel 7 site. Plumes exhausting into this wind environment were lofted quite high by their initial momentum; hence, they rarely penetrated the local wake region, and the plume touched down farther downwind.

Winds from the SE direction passed over only low rise residential areas before reaching the Parcel 7 site. High wind speeds at stack height deflected the plume immediately; hence, downwash was often significant behind the Government Center garage. Furthermore, even plumes which did not reach ground level quickly often impacted the tall skyscrapers which stand to the NW. Such conditions will result in maximum concentrations at elevated samplers located on roof tops.

Winds from the WSW channeled their way along Sudbury Street in the commercial district. The resulting high winds appeared to cause a low pressure region behind the JFK Federal Building which shifted the wind over the Parcel 7 site toward the E. Often these winds produced vent plume downwash which resulted in a groundlevel plume extending eastward over the eastern part of the Boston peninsula.

Conclusions from Smoke Visualization Tests:

The visualization tests provided observations which permitted focus for the concentration experiments. The major conclusions were:

1. For a given exit flow velocity, wind speed and site orientation, the higher the stack, the lower the ground smoke concentration.

2. Vent exit velocities which exceeded 1.5 times the reference wind speed reduced stack and building downwash. Consequently exit velocities 1600 ft/min and greater were more desireable than the 800 ft/min flow velocity.

3. The roof space available on top of the Parcel 7 building was not great enough to permit significant separation of the individual vents. Varying stack grouping did not produce noticeable differences in smoke concentration on the ground.

4. A tall stack and short building is the most desirable combination to avoid local building downwash. A tall building with a short stack will always result in some downwash to street level. Short buildings result in large ground level concentrations because the plume is mixed over a smaller building cavity; whereas a taller building will produce a larger cavity region to dilute the gas plume. Based on qualitative evaluation of the smoke visualization results concentration measurements focused on building heights greater than or equal to 75 feet and stack heights greater than or equal to 125 feet.

5. Adjacent garage heights ranging from 42 to 90 feet did not produce great differences in plume behavior. Surface smoke was somewhat greater for 75 foot garage buildings attached to a 75 foot Parcel 7 building.

6. The WSW and SE wind directions were identified as critical directions having the potential for high concentrations.

5.2. VERIFICATION OF FLUID MODEL RELIABILITY

Similarity of flow and dispersion of gas plumes over the Boston city complex must exist to obtain reliable estimates of concentrations. Appendix Section A.2.1 notes that equivalence is generally assured if the characteristic Reynolds number (or model velocity) is sufficiently large. Concentration test runs 15 through 25 were performed to determine the minimum tunnel wind speed at which the K coefficients did not vary. Although runs were performed over a five-fold range in magnitude of wind speeds and ventilator flow rates, the ratio of exhaust velocity to wind speed was held constant at 0.81. Thus, sample point concentrations in terms of ppm or K coefficient should remain constant if similarity holds. Figure 22 displays resulting concentrations in terms of K for the WSW wind orientation. Data for the NNE and S wind directions behaved similarly (see Figure 23 and Figure 24). Note that all values for prototype

reference wind speeds greater than 5 m/s are equivalent; whereas the values are less for a prototype wind speed of 2.5 m/s. Since Reynolds number independence holds for wind speeds at 5 m/s and greater, all subsequent test runs were performed at prototype wind speeds of 5 m/s or greater.

5.3. BUILDING AERODYNAMICS EFFECTS ON PARCEL 7 VENTILATOR PLUMES

Test Runs 53 to 56 were performed with a 125 ft stack located on the Parcel 7 site in place of the proposed building and ventilator system. These data may be compared with Runs 4, 7, 38, and 41 to determine the influence of building downwash on plume concentrations. Figure 25 displays typical results for the SE wind direction. Note that when the Parcel 7 structure is present concentrations are often ten times larger. The building has reduced the effective plume release height by deflecting the plume toward the ground resulting in larger concentrations. Depending upon the resultant plume trajectory elevated concentrations may be either smaller or greater.

The Boston city complex which surrounds the Parcel 7 site will also influence plume trajectories and mixing rates. The plume can stagnate on tall buildings, deflect around tall buildings, or be diverted into street canyons or between buildings by local low pressure regions. The buildings also produce a complex structure of turbulence and wake regions which can dilute the plume or mix it toward the ground. These effects can sometimes mask the effect of the source building upon the exhaust plume. Test Runs 57 through 60 were performed with the Boston city model removed from the wind tunnel. Data were measured at ground level on crosswind trajectories located at distances of 256, 1664 and 2369 feet downwind of the Parcel 7 ventilators. Wind orientations considered were N, E, SE and SW. Figure 26, Figure 27 and Figure 28 display typical cross-wind concentration distributions at 256, 1664 and 2369 feet respectively. At 256 feet the patterns suggest that maximum downwash occurs for easterly winds, whereas maximum plume deflection occurs for south-westerly winds. At 2369 feet downwind the plumes appear uniformly distributed, and only the easterly results show the effects of downwash.

5.4. INFLUENCE OF ALTERNATIVE STACK CONFIGURATIONS UPON CONCENTRATIONS

Given no other controlling factors (such as zoning regulations or cost) it is evident minimum surface concentrations will occur for maximum stack height, minimum building height, and maximum exhaust velocity. In order to avoid all building aerodynamic effects, wind engineers recommend releasing plumes stacks at elevations greater than or equal to 2.5 times the minimum of building height or width. In the case of a 75 foot Parcel 7 ventilation building this would require an effective stack height greater than 188 feet. Shorter stacks permit plume interaction with the separation cavity which forms about the building, and, consequently, larger surface concentrations occur.

Effect of Variations in Stack Height:

Figure 29 compares sampler concentrations for the SE wind direction for stack heights varying from 100 to 225 feet with an exhaust gas velocity of 1600 fpm (Runs 2, 4, 8, and 12). Figure 30 compares sampler concentrations for the WSW wind direction for similar conditions (Runs 1, 3, 6, and 11). Taller stacks generally produce smaller sampler concentrations, but the 75 foot tall building and garage complex tends to produce some plume downwash for all the stacks shorter than 225 feet. Given a restriction to stack heights less than 150 feet, concentrations are all of the same order of magnitude.

Effects of Variations in Exhaust Velocity:

Significant reductions in sample point concentrations can be obtained by increasing stack gas velocity. Figure 31 compares sampler concentrations from a 125 foot stack for the SE wind direction for exhaust velocities varying from 400 to 3200 fpm (Runs 4, 46, 47 and 48). Figure 32 compares sampler concentrations for the WSW wind direction for similar conditions (Runs 3, 43, 44, and 45). Figure 33 and Figure 34 display similar data for the NNE and ENE wind directions. Figure 35 compares sampler concentrations for the SE wind direction but from a 150 foot stack (Runs 6, 8, and 10). A four-fold increase in stack velocity produces about a six-fold decrease in concentration, whereas an eight-fold increase in stack velocity produces about a twenty-fold decrease in concentration. Stack downwash may occur for exhaust velocity to wind speed ratios less than 1.5. For the Parcel 7 complex a 5 m/sec wind speed the 400 and 800 fpm conditions permit significant stack downwash ($W/U < 1$); whereas, downwash is usually absent at large exhaust velocities ($W/U \geq 1.6$).

Joint Influence of Stack Height and Exhaust Velocity:

Consideration of smoke visualization and concentration results suggests that a 125 foot stack height with an exit flow velocity of 1600 ft/min is the lowest stack height and exit flow velocity reasonable for the Parcel 7 vent building. This stack height and exhaust velocity should suffice to avoid stack downwash and loft the ventilator plume above the building cavity for wind speeds below 5 m/sec.

Influence of Building Orientation:

Wind orientation combines with building orientation, building and stack downwash, exhaust velocity and sample location to produce a wide variance in sample concentrations. Figure 36, Figure 37 and Figure 38 consider sample location concentration variation for a 125 ft stack exhausting at 1600 fpm in a 5 m/sec wind. Maximum K concentrations lie between 3 to 4 x 10^{-6}. These concentrations can occur for winds from the N, NE, SE, SW and W.

APPENDIX: MODELING OF PLUME DISPERSION

To obtain a predictive model for a specific plume dispersion problem, one must quantify the pertinent physical variables and parameters into a logical expression that determines their inter-relationships. This task is achieved implicitly for processes occurring in the atmospheric boundary layer by the formulation of the equations of conservation of mass, momentum and energy. These equations with site and source conditions and associated constitutive relations are highly descriptive of the actual physical interrelationship of the various independent variables (space and time) and dependent variables (velocity, temperature, pressure, density, concentration, etc.).

These generalized conservation statements subject to the typical boundary conditions of atmospheric flow are too complex to be solved by present analytical or numerical techniques. It is also unlikely that one could create a physical model for which exact similarity exists for all the dependent variables over all the scales of motion present in the atmosphere. Thus, one must resort to various degrees of approximation to obtain a predictive model. At present, purely analytical or numerical solutions of boundary layer, wake, and plume dispersion are unavailable because of the classical problem of turbulent closure (Hinze, 1975). However, boundary layer wind tunnels are capable of physically modeling plume processes in the atmosphere under certain restrictions. These restrictions are discussed in the next sections.

A.1 FLUID MODELING OF THE ATMOSPHERIC BOUNDARY LAYER

The atmospheric boundary layer is that portion of the atmosphere extending from ground level to a height of approximately 1000 meters within which the major exchanges of mass, momentum, and heat occur. This region of the atmosphere is described mathematically by statements of conservation of mass, momentum and energy (Cermak, 1975). The mathematical requirements for rigid laboratory/atmospheric-flow similarity may be obtained by fractional analysis of these governing equations (Kline, 1965). This methodology scales the pertinent dependent and independent variables by size and then casts the equations into dimensionless form by dividing by one of the coefficients (the inertial terms in this case). Performing these operations on such dimensional equations yields dimensionless parameters commonly known as:

Reynolds number	$Re = (UL/\nu)_r$	=	$\frac{\text{Inertial Force}}{\text{Viscous Force}}$
Bulk Richardson number	$Ri = [(Lg\Delta T/T)/U^2]_r$	=	$\frac{\text{Gravitational Force}}{\text{Inertial Force}}$
Rossby number	$Ro = (U/L\Omega)_r$	=	$\frac{\text{Inertial Force}}{\text{Coriolis Force}}$

Prandtl number $Pr = [\nu/(k/\rho C_p)]_r$ = $\frac{\text{Momentum Diffusivity}}{\text{Thermal Diffusivity}}$

Eckert number $Ec = [U^2/C_p\Delta T]_r$

A.1.1 Exact Similarity

For exact similarity between flows which are described by the same set of equations, each of these dimensionless parameters must be equal for both flow systems. There must also be similarity between the surface-boundary conditions and the approach flow wind field. Surface-boundary condition similarity requires equivalence of the following features:

a. Surface-roughness distributions,
b. Topographic relief, and
c. Surface-temperature distribution.

If all the foregoing requirements are met simultaneously, all atmospheric scales of motion ranging from micro- to mesoscale could be simulated within the same flow field. However, all of the requirements cannot be satisfied simultaneously by existing laboratory facilities; thus, a partial or approximate simulation must be used. This limitation requires that atmospheric simulation for plume dispersion must be designed to simulate most accurately those scales of motion which are of greatest significance for the transport and dispersion of plumes.

A.1.2 Partial Simulation of the Atmospheric Boundary Layer

For many fluid modeling situations several of the aforementioned parameters are unnecessarily restrictive and may be relaxed without causing a significant loss in similarity between model and field fluid flow. The Rossby number magnitude controls the extent to which the mean wind direction changes with height. The effect of Coriolis-force-driven lateral wind shear on wind flow is only significant when heights are of the same order of magnitude as the boundary layer height. The Eckert number (in air $Ec = 0.4\ Ma^2\ (T_r/\Delta T_r)$, where Ma is the Mach number) is the ratio of energy dissipation to the convection of thermal energy. Both in the atmosphere and the laboratory flow, the wind velocities and temperature differences are such that the Eckert number is very small; hence, it is neglected. Prandtl number equality guarantees equivalent rates of momentum and heat transport. Since air is the working fluid in both the atmosphere and the laboratory, Prandtl number equality is always maintained.

The approach flow Richardson number (Ri) and Reynolds number (Re) determine the kinematic and dynamic structure of turbulent flow within a boundary layer. This influence is apparent in the variations that occur in the spectral distribution of turbulent kinetic energies with changing Ri and changing Re.

The Reynolds Number

Re equality implies $U_m = (L_p/L_m)U_p$. Re equality at a significantly reduced length scale would cause the model's flow velocity to be above sonic; hence, its equality must be distorted. A reduced Re changes only the higher frequency portion of an Eulerian-type description of the spectral energy distribution. Unfortunately, there is no precise definition as to which portion of an Eulerian Spectrum is dominant in dispersing ground-level or elevated plumes over moderate travel distances.

Most investigators use a minimum Reynolds number requirement based on rough-walled pipe measurements; i.e., $Re = u_* z_o/\nu > 2.5$, where u_*, the friction velocity, and z_o, the roughness length, are derived from a log-linear fit to a measured mean velocity profile. The value 2.5 is an empirically determined constant. At Re below 2.5, it is observed that the mean velocity profiles in turbulent pipe flow lose similarity in shape and deviate from the universal curve of a rough wall turbulent boundary layer. For Re above 2.5, it is observed that the surface drag coefficient (and thus the normalized mean velocity profile) is invariant with respect to increasing Re. For Re between 0.11 and 2.5, the velocity profiles are characteristic of smooth wall turbulent boundary layers. For values below 0.11, the growth of a laminar sublayer on the wall is observed to increase with decreasing Re.

Extrapolation of results from pipe flow measurement to flat plate boundary layers may cause a shift in the magnitude of the minimum Re requirement, but it is generally felt that this shift is small. Precise similarity in the universal form of mean wind shear may be necessary for invariance with respect to the surface drag coefficient, but this does not necessitate that precise similarity must exist for the invariance of the wind field and dispersion. It is the distribution of turbulent velocities which has the greatest effect on the wind field and dispersion. It is the mean wind shear, however, which generates the turbulent velocities. It is possible that the specification of a minimum Re of 2.5 is overly conservative. The criteria, $Re > 2.5$, for example, is not applicable for flow over complex terrain or building clusters.

The Richardson Number

Although most wind-tunnel investigations are conducted with neutrally stratified boundary layers, there are circumstances when the stratification of the atmosphere must be considered. In particular, air pollution and dispersion problems are often critical during stratified conditions. Unstable stratification may be expected to mitigate hazards by accelerating plume dilution, whereas stable stratification may permit high concentrations to persist. The stability state of the atmosphere is typically characterized by the Richardson number.

The atmospheric gradient Richardson number can be computed from averaged quantities through the equation

$$Ri = g/T\ (\Gamma_d - \Gamma)\ [1 + 0.07/B]\ [(\partial u/\partial z)^2 + (\partial v/\partial z)^2]$$

where Γ and Γ_d are the actual and dry adiabatic potential temperature lapse rates, and $B = [C_p(T_2-T_1)]/[(Z_2-Z_1)(Q_2-Q_1)]$ is the Bowen ratio of sensible to latent heat flux at the surface. The Ri number can be taken to represent the ratio of the relative importance of convective and mechanical turbulence. Negative Ri numbers of large value indicate strong convection and weak mechanical turbulence; zero Ri numbers imply purely mechanical turbulence. Positive Ri numbers less than some critical value, $Ri_{critical}$, suggest the presence of mechanical turbulence damped by the density-induced buoyancy forces; for larger positive Ri numbers, turbulence essentially disappears, since the stratification overpowers production by wind shear. The critical Richardson number has a value near 0.25.

A.1.3 Performance of Prior Fluid Modeling Experiments

Meroney et al. (1978) summarized experimental data available from field and laboratory studies for neutral airflow over hills, ridges, and escarpments. Wind-tunnel model measurements were performed to study the influence of topography profile, surface roughness and stratification on the suitability of various combinations of these variables. Detailed tables of velocity, turbulence intensity, pressure, spectra, etc., were prepared to guide numerical model design and experimental rule of thumb restrictions. Cases included hill slopes from 1:2 to 1:20, neutral and stratified flows, two- and three-dimensional symmetric ridges, six alternate hill and escarpment shapes, and a variety of windward versus leeward slope combinations to evaluate ridge separation characteristics. The laboratory data were validated by comparison with field measurements for flow in the Rakaia Gorge, New Zealand, and over Kahuku Point, Oahu, Hawaii, (Meroney et al., 1978; Chien, Meroney and Sandborn, 1979).

Local heating and cooling of coastline or hill surfaces are the driving mechanisms for sea-land breezes, and anabatic and katabatic winds which may inhibit or enhance airflow over the land surface. Early laboratory work includes simulations of urban heat islands by Yamada and Meroney (1971) and Sethuraman and Cermak (1973), simulation of flow and dispersion at shoreline sites by Meroney et al. (1975a), and simulation of dispersion effects of heat rejected from large industrial complexes by Meroney et al. (1975b).

Meroney (1980) compared three model/field investigations of flow over complex terrain, suggested performance envelopes for realizable modeling in complex terrain, and discussed recent laboratory studies which provide data for valley drainage flow situations. Not all of the model/field comparison experiments performed in the past were successful. Many early studies had model approach flow velocity exponents near zero, were modeled as neutral flows when the field observed strong stratification effects, or simulated unrealistic boundary layer depths, integral scales, or turbulence intensities which did not match their atmospheric counterpart. But few studies claimed unreasonable correlation, and some were strongly self-critical. Nonetheless, most studies accomplished their prestated limited objectives. It would appear that the simulation hypothesis developed in the last few years is

appropriate for physical modeling of flow over complex terrain when appropriate care is taken to simulate the approach flow conditions and to maintain simulation parameters equal between model and prototype.

Arya and Plate (1969), Arya (1975) performed velocity, temperature, and turbulence measurements in the lowest 15 percent of a 70 cm deep boundary layer over a smooth surface, where conditions ranged from unstable to moderately stable ($-0.3 < z/L_{mo} < 0.3$). Free stream flow speeds varied from 3 to 9 m/s, and temperature differences were about 40°C across the boundary layer. Cermak, Shrivastava and Poreh (1983) reported mean velocity and turbulence measurements made for a variety of simulated atmospheric boundary layers over different surface roughness. Free stream flow speeds varied from 2.4 to 3.0 m/s and temperature differences were from 150°C to -80°C across the boundary layer. Poreh and Cermak (1984) reproduced unstable lapse conditions including mixed layers and elevated inversions. They reproduced the characteristics of convective boundary layer turbulence measured in the atmosphere.

Diffusion studies made by Chaudhry and Meroney (1973) in stable boundary layers investigated previously by Arya (1969) have shown agreement of experimental results with Lagrangian similarity theory. Horst (1979) tested Lagrangian similarity predictions of crosswind-integrated ground concentration against the Prairie Grass diffusion experiment (Barad, 1958) and an experiment at Idaho Falls (Islitzer and Dumbauld, 1963). He reported good agreement for all stabilities at distances x/z_o out to $2*10^5$. Poreh and Cermak (1984, 1985) released plumes in their modeled mixing layer. Their plumes exhibited the plume lofting typical of ground sources and the descent typical of elevated sources, predicted from water tank experiments by Willis and Deardorff (1974, 1976, 1978) and numerically by Lamb (1982).

Staff at the Fluid Mechanics Laboratory at the Ecole Centrale de Lyon have studied unstable wind-tunnel boundary layers and compared them with the atmospheric boundary layer (Schon and Mery, 1971). Flow speeds were typically 2 to 4 m/s and the floor temperature was maintained 50°C above ambient. Comparisons with the Kansas data (Haugen et al., 1971) were quite satisfactory, but longitudinal turbulence intensities exhibited a slight Reynolds number dependence, and spectral energy was too low in the high frequency portions of the spectra. The most unstable flow they studied had a Monin-Obukhov scale length of about -1 m at model scales, or -500 to -1000 when scaled to the atmosphere.

A.2 PHYSICAL MODELING OF BLUFF BODY AERODYNAMICS

The interaction of an approach wind field with bluff bodies or structures constructed on the earth's surface is broadly termed "Building Aerodynamics." In a review article on this subject, Meroney (1982) discusses the character of bluff body flow about rectangular buildings and cylindrical cooling towers. Defects in velocity profiles can easily persist from 10 to 15 building heights downwind. Field and laboratory measurements of plume dispersion about the Rancho Seco Nuclear Power Station in Sacramento, California, confirm that cooling tower wake effects

persist for significant downwind distances under a variety of stratification conditions (Allwine, Meroney and Peterka, 1978; Kothari, Meroney and Bouwmeester, 1981).

A.2.1 Simulation Criteria

Often atmospheric turbulence may cause only weak effects compared to the turbulence generated by buildings, obstacles, and terrain. Yet the magnitude of the perturbations depends upon the incident flow turbulence scale and intensity, details of the obstacle shape and surface roughness, and size of the obstacle compared to the boundary layer depth. Geometrical scaling implies that the ratio of the building height to length scale must be matched and, of course, that all other building length scales be reduced to this same ratio.

Several questions should be considered when modeling flows which include surface obstacles:

a. What size obstacles should be disregarded?
b. What detail or roughness on an obstacle need be included?
c. To what upwind distance should all obstacles be included?
d. At what point does the size of a modeled obstacle become too big for the wind tunnel (i.e., blockage effects)?
e. What is the effect on the flow field of mismatching obstacle and approach flow length scales?
f. What is the minimum allowable model obstruction Reynolds number?

Obstacle sizes to be disregarded:

Boundary layer studies of rough surfaces reveal that if protuberances are of a size k, such that $u_*k/\nu < 5$, they will have little effect on the flow in a turbulent boundary layer. Thus, assuming a laboratory wind speed of 1 m/s and a typical friction coefficient $C_f/2 = (u_*/u)^2 = 0.0025$, obstacles of size less than 2 mm would go unnoticed.

Required obstacle surface detail or roughness:

Another question that always arises is "How much detail is required for the building or obstacle model? The answer is, of course, dependent upon the size of the protuberance compared to the plume and the dominant eddies of mixing. If the obstruction is large enough to modify the separated wake over the main obstacle, then it must be included. Often an equivalent obstacle surface roughness suffices. Snyder (1981) concludes a generic surface roughness criterion might be $u_*k/\nu > 20$. For a 1 m/s laboratory flow this results in model roughness elements equal to about 6 mm. But since the exterior flow is usually highly turbulent, the body typically includes a highly unsteady wake, and the u_* value to be used should be that acting on the building surface, rather than that of the approach flow. Hence, even this roughness may be unnecessarily large.

Upstream fetch to be modeled:

Suppose there is another building, tree line, fence, cooling tower, or obstacle some distance, s, upstream of a meteorological measurement location; is it necessary to include this obstacle in the wind-tunnel

model? Hunt (1974) showed that the velocity deficit in the wakes of cubes and cylinders is given approximately by:

$$DU_{mx}/U(h) = A\ (s/h)^{-3/2}$$

downwind of the separation bubble, where DU_{mx} is the maximum mean velocity deficit created by the obstacle, h is the height of the obstacle, S is the distance downstream of the obstacle, and A is a constant dependent upon the obstacle shape, orientation, boundary layer thickness, etc. Typically, A = 2.5, but it may range from 1.5 to 5.0. If we desire that the velocity at the spill site be within 3 percent of its undisturbed value, Snyder (1981) recommends that any upstream obstacle as high as s/20 be included upstream in the model of the spill site. If the obstacle's width is much greater than its height (for example, a fence or ridge), one should include it in the physical model if its height is greater than s/100.

Blockage effects:

Because of the influence of wind-tunnel walls on the behavior of the flow past models, it is desirable to use small models or big tunnels, or both. On the other hand, larger models are not only easier to work with, but they may be needed for similarity reasons to achieve large enough Reynolds numbers. It is possible to identify three different types of effects of wind-tunnel constraints. The first is the simple "solid blockage" effect which arises because the fluid stream is unable to expand laterally as it normally would in unconfined flow. The second effect, called "wake blockage", results because the accelerated flow between an obstacle and the tunnel walls continues to "pinch" the wake flow region and reduce its normal lateral rate of growth. The third effect is produced by the growth of boundary layers on the tunnel walls which produce "wall boundary interference." Tunnel blockage can cause separation and reattachment locations to vary, produce higher velocities, larger wake turbulence, and modify the dispersion patterns in the vicinity of obstructions.

The ratio of the cross-sectional area of a model obstacle to that of the tunnel is called the "blockage ratio", BR. Mass continuity produces an average velocity speed-up of S = BR/(1-BR). Although wind tunnels with adjustable ceilings can compensate to some extent by raising the roof locally; this is not a perfect solution to the problem. Measurements on building and cooling tower models placed in different size wind-tunnel test sections reveal major changes in the character of pressure distributions, separation, and wake growth in the presence of flow restricted by wind-tunnel side walls (Farell et al., 1977).

Blockage corrections, which are conventionally applied in aeronautical tunnels, cannot usually be applied to the typical asymmetric model configuration placed against the wall of a meteorological wind tunnel (Ranga Raju and Singh, 1976). Conventional wisdom now suggests the "rule of thumb" that blockage ratios greater than five percent should be avoided.

Simulation of the flow over sharp-edged obstacles:

A number of authors have discussed flow studies about simple cubical or rectangular sharp-edged obstacles. An extensive review about such flow fields and the subsequent character of diffusion near obstacles has been provided by Hosker (1984). Peterka, Meroney and Kothari (1985) describe typical flow deviations which result from the presence of a sharp-edged building.

Consider the main features of the flow around a sharp-edged building. Typically, when the approach flow is normal to the building face, the flow separates from the ground upwind of the building and produces a "horseshoe"-shaped vortex which wraps around the base of the building. The surface streamline reattaches on the front of the building, and fluid parcels move up and down the building's forward face. An elevated streamline flows over the obstacle, dips down behind, and stagnates on the surface at the end of the recirculating cavity immediately downwind of the building. Sometimes separation streamlines from the forward building edges reattach to the same face, yet in other cases the streamlines enter the downwind cavity and mingle with the other recirculating fluid. Air which enters the cavity departs through turbulent mixing across the dividing streamlines, mingles with downwind-pointing vortices and is ejected laterally out of the cavity, or leaves suddenly during an exhalation when the entire cavity appears to collapse and then reform.

When a building is oriented obliquely to the wind, flow over the front side walls does not separate, but strong recirculation occurs on the downwind faces. Flow over the roof often produces counter-rotating "delta-wing" vortices which increase mixing over the top and in the wake of the building. These vortices can cause reattachment of the flow in the middle of the roof and serious plume downwash in the near wake. Other features of the flow near the building include vertical vortices produced by the vertical corners of the building.

Golden (1961) measured the concentration patterns above the roof of model cubes in a wind tunnel. Two sizes of cubes were used to vary the Reynolds number from 1000 to 94,000. The concentration isopleths in the fluid above the cube roof showed only slight variations over the entire range of Reynolds numbers studied. The maximum concentration on the roof itself was found to vary strongly with Reynolds numbers less than 11,000, but to be invariant with Reynolds numbers between 11,000 and 94,000. Frequently, modelers quote Golden's experiments as justification for presuming dispersion invariance when obstacle Reynolds numbers exceed 11,000. However, Golden's "11,000 rule" is limited to the measurement of concentrations at only one point on the roof of smooth-walled cubes placed in a uniform approach flow of very low turbulent intensity. It is probably quite conservative because the shear and high turbulence in a simulated atmospheric boundary layer are likely to further reduce the critical Reynolds number. Indeed, Halitsky (1968) observed that for dispersion in the wake region, no change in isoconcentration isopleths

from passive gas releases was found to occur for values of Reynolds number as low as 3300.

Flow around sharp-edged obstacles will remain kinematically similar at very low Reynolds numbers. Wake width variation will be minimal, and obstacle generated turbulence scales and intensity will only vary slowly as Reynolds number decreases. Gas clouds dispersing in this environment will remain similar at very low model speeds.

Simulation of flow over rounded obstacles:

Flow around a smooth cylinder is Reynolds number dependent. This dependence reflects changes in the nature of the boundary layer that forms over the cylinder and its behavior in the vicinity of the flow separation. At low Reynolds numbers, the boundary layer is laminar, and separation occurs easily under the influence of even modest positive pressure gradients. At higher Reynolds numbers, the boundary layer becomes turbulent and flow separation is delayed; i.e., the flow can move farther along a curved surface without separation. At prototype scales, obstacles are large enough that only turbulent separation occurs. However, model flows are usually at such low Reynolds numbers that the local boundary layer growing over a curved surface would be laminar. Most modelers attempt the reproduction of full- scale similarity around curved surfaces by artificially roughening the model surface to force transition to turbulence in these laminar boundary layers. This can be done by providing the surface with special (or artificial) roughness elements, for example, sandpaper, thin wires, or grooves. The height of the roughness, k, should be such that $Uk/\nu > 400$ and $k/R < 0.01$, where U is the mean wind speed at obstacle height, and R is the characteristic obstacle radius of curvature. Szechenyi (1975) studied flows about rough circular cylinders and determined that as Reynolds number decreases, roughening the surface becomes less effective. Fage and Warsap (1929) considered the effect of increasing the surface roughness of cylinders on their drag coefficient. Eventually, even ridiculously large roughness is ineffective.

Niemann and Ruhwedel (1980) compared pressures and forces about a 1:333 scale model to a full-scale hyperbolic cooling tower shell. They roughened their model with vertical ribs of height 0.09 mm and width 0.77 mm, producing a roughness coefficient of $k/2R = 0.0006$ and roughness Reynolds number, $Re_k > 270$. They found meridional forces on the cooling tower model and prototype were similar. Model Reynolds numbers were between $4.5*10^5$ and $6.0*10^5$, and this corresponding to $U_m > 45$ m/s. But again these speeds are much higher than is appropriate for current measurements.

Halitsky et al. (1963) examined dispersion about a smooth-model nuclear reactor containment building (a hemisphere fitted on a vertical cylinder) and found a critical Reynolds number greater than 79,000. (Yet this critical Reynolds number was for flow very close to the vessel wall. The behavior of concentration isopleths further downwind is likely to be less Reynolds number dependent.)

Although the details of fluid motions around rounded obstacles vary significantly with Reynolds number, the gross features of the flow do not change. Even small models at low wind speeds will produce horseshoe-shaped ground vortices, elevated pairs, and regular vortex shedding. If the internal boundary layer over the obstacle is laminar, then the wake region will be broader and less intense.

A.2.2 Performance of Prior Fluid Modeling Experiments

A number of studies have been performed in the Colorado State University Fluid Dynamics and Diffusion Laboratory to establish the effect of buildings and meteorological masts on flow fields. Hatcher et al. (1977) examined flow and dispersion in stratified flow downwind of the Experimental Organic Cooled Reactor, Idaho Falls; Allwine et al. (1978) studied the Rancho Seco Reactor, Sacramento; Kothari et al. (1981) studied the Duane Arnold Energy Center, Iowa. In each case field measurements were compared to laboratory measurements with good agreement. Specific effects of the structure of a meteorological mast on instrumentation response were reported by Hsi and Cermak (1965).

A.3 PHYSICAL MODEL OF PLUME MOTION

In addition to modeling the turbulent structure of the atmosphere in the vicinity of a test site it is necessary to properly scale the plume source conditions. One approach would be to follow the methodology used in Section 2.1; i.e., writing the conservation statements for the combined flow system followed by fractional analysis to find the governing parameters. An alternative approach, the one which will be used here, is that of similitude (Kline, 1965). The method of similitude obtains scaling parameters by reasoning that the mass ratios, force ratios, energy ratios, and property ratios should be equal for both model and prototype. When one considers the dynamics of gaseous plume behavior the following nondimensional parameters of importance are identified.[1]

$$\text{Mass Flux Ratio} = \frac{\text{mass flow of plume}}{\text{effective mass flow of air}}$$

$$\text{Momentum Flux Ratio} = \frac{\text{inertia of plume}}{\text{effective inertia of air}}$$

$$\text{Densimetric Froude No. (relative to the inertia of the air)} = \frac{\text{effective inertia of air}}{\text{buoyancy of plume}}$$

[1] The scaling of plume Reynolds number is also a significant parameter. Its effects are invariant over a large range. This makes it possible to accurately model its influence by maintaining model tests above a minimum plume Reynolds number requirement.

Densimetric Froude No. (relative to the inertia of the plume) = $\frac{\text{inertia of plume}}{\text{buoyancy of plume}}$

Flux Froude No. = $\frac{\text{momentum flux of air}}{\text{buoyancy momentum flux of plume}}$

Volume Flux Ratio = $\frac{\text{volume flow of plume}}{\text{effective volume flow of air}}$

It is necessary to maintain equality of the plume's specific gravity, ρ_g/ρ_a, over the plume's entire lifetime to obtain simultaneous simulation of all of these parameters. Unfortunately a requirement for equality of the plume gas specific gravity for plume with significant buoyancy differences (i.e. ρ_g not equal ρ_a) leads to several complications in practice. These are:

1) Equality of the source gas specific gravity between a model and its atmospheric equivalent leads to a wind speed scaling from $(U_m/U_p)^2 = L_m/L_p$. For a significant range of atmospheric wind speeds this relationship leads to wind- tunnel speeds at which there is a possible loss of the Reynolds number invariance in the approach flow.

2) A thermal plume in the atmosphere is frequently simulated in the laboratory by an isothermal plume formed from a gas of appropriate molecular weight. Under certain situations of specific heat capacity mismatch, this practice will lead to a variation of the equality of plume density as the plume mixes with air.

It is important to examine each modeling situation and decide if an approximation to complete plume behavior may be employed without a significant loss in the similarity of the modeled plume structure.

REFERENCES

Allwine, K. J., Meroney, R. N., and Peterka, J. A. (1978), "Rancho Seco Building Wake Effects on Atmospheric Diffusion: Simulation in a Meteorological Wind Tunnel," FDDL Report No. CER77-78KJA-RNM-JAP25, Colorado State University, Fort Collins, Colorado.

Arya, S. P. S., and Plate, E. J. (1969), "Modeling of the Stably Stratified Atmospheric Boundary Layer," J. Atmos. Sci., Vol. 26, No. 4, pp. 656-665.

Ayra, S. P. S. (1975), "Buoyancy Effects in a Horizontal Flat-Plate Boundary Layer," J. Fluid Mech., Vol. 68, Pt. 2, pp. 321-343.

Barad, M. L., Ed. (1958), Project Prairie Grass: A Field Program in Diffusion, Geophysical Research Papers, No. 59, Vols. I and II, Report AFCRC-TR-58-235, Air Force Cambridge Research Center.

Brunn, (1978), "Multi-Probes and Higher Moments," Proceedings of the Dynamic Flow Conference 1978, pp. 943-961.

Cermak, J. E. (1975), "Applications of Fluid Mechanics to Wind Engineering--A Freeman Scholar Lecture," J. of Fluids Engineering, Vol. 97, pp. 9-38.

Cermak, J. E., Shrivastava, P. K., and Poreh, M. (1983), "wind-tunnel Research on the Mechanics of Plumes in the Atmospheric Surface Layer," Civil Engineering Department Report CER83-84JEC-PKS-MP12, Colorado State University, Fort Collins, CO, Annual Progress Report to U.S. Dept. of Army Contract DAAK11-82-K-0004, 140 pp.

Chaudhry, F. H. and Meroney, R. N. (1973), "A Laboratory Study of Diffusion in Stably Stratified Flow," Atmos. Envir., Vol. 7, pp. 443-454. Chien, H. C., Meroney, R. N., and Sandborn, V. A. (1979), "Sites for Wind-Power Installations: Physical Modeling of the Wind Field Over Kahuku Point, Hawaii," FDDL Report No. CER79-80HCC-RNM-VAS25, Colorado State University, Fort Collins, Colorado.

Counihan, J. (1975), "Adiabatic Atmospheric Boundary Layers: A Review and Analysis of Data from the Period 1880-1972," Atmos. Envir., Vol. 9, pp. 871-905.

Fage, A. and Warsap, J. H. (1929), "Effects of Turbulence and Surface Roughness on Drag of Circular Cylinders," U.K., ARC R&M 1283.

Farell, C., Carrasquel, S., Guven, O., and Patel, V. C. (1977), "Effect of Wind-Tunnel Walls on the Flow Past Circular Cylinders and Cooling Tower Models," J. of Fluids Engineering, Vol. 99, pp. 470-479.

Gifford, F. A. (1976), Turbulent Diffusion-Typing Schemes: A Review, Nucl. Saf., Vol. 17, No. 1, pp. 72 ff.

Golden, J. (1961), "Scale Model Techniques," M.S. Thesis, Dept. of Met. and Ocean., New York University, 42 pp.

Golder, D. G. (1972), "Relations Among Stability Parameters in the Surface Layer," Boundary-Layer Meteorol., Vol. 3, No. 1, pp. 47-58.

Halitsky, J., Colden, J., Halpern, P., and Wu, P. (1963), "Wind Tunnel Tests of Gas Diffusion from a Leak in the Shell of a Nuclear Power Reactor and from a Nearby Stack," N.Y.U. Meteorol. and Oceanog. Geophys. Sciences Lab. Report 63-2 (New York Univ., College of Engineering, New York.)

Halitsky, J. (1968), "Gas Diffusion Near Buildings," Meteorology and Atomic Energy, 1968, editor D. H. Slade, Atomic Energy Commission, Ch. 5-5, pp. 221-256.

Hatcher, R. V. and Meroney, R. N. (1977), "Dispersion in the Wake of a Model Industrial Complex," Joint Conf. on Applications of Air Pollution Meteorology, Proceedings, Am. Meteorol. Sco., Salt Lake City, Utah, 29 November - 2 December, 1977, pp. 343-346.

Haugen, D. A., Kaimal, J. C., and Bradley, E. F. (1971), "an Experimental Study of Reynolds Stress and Heat Flux in the Atmospheric Surface Layer," Quart. J. Roy. Meteorol. Soc., Vol. 97, pp. 168-180.

Hinze, J. O. (1975), Turbulence, McGraw-Hill, New York, 2nd. edition, 790 pp.

Horst, T. W. (1979), "Lagrangian Similarity Modeling of Vertical Diffusion from a Ground Level Source," J. Appl. Meteorol., Vol. 18, pp. 733-740.

Hosker, R. P., Jr. (1984), "Flow and Diffusion Near Obstacles," Atmospheric Science and Power Production, DOE/TIC-27601, pp. 241-326.

Hsi, G., and Cermak, J. E. (1965), "Meteorological-Tower Induced Wind Field Perturbations," Prepared under U.S. Army Research Grant DA-AMC-28-043-64-G-9, Fluid Mechanics Program Report No. CER65GH-JEC49, Colorado State University, Fort Collins, Colorado.

Hunt, J. C. R. (1974), "Wakes Behind Buildings," presented at the Aeronautical Research Council's Atmospheric Environment Committee Meeting, Oct. 23, ARC Report 35601, Atmos. 229, Aeronautical Research Council of Great Britain, Her Majesty's Stationery Office, London.

Hunt, J. C. R., Snyder, W. H., and Lawson, F. E., Jr. (1978), "Flow Structure and Turbulent Diffusion around a Three-Dimensional Hill: Fluid Modeling Study on Effects of Statification: Part I: Flow Structure," Envir. Prot. Agcy. Report No. EPA 600/4-78-041, Fesearch Triangle Park, NC, 84 pp.

Islitzer, N. F. and Dumbauld, R. K. (1963), "Atmospheric Diffusion Deposition Studies over Flat Terrain," INt. J. Air Water Pollut., Vol. 7 (11-12), pp. 999-1022.

Kline, S. J. (1965), Similitude and Approximation Theory, McGraw-Hill Book Company, New York, 229 pp.

Kothari, K. M., Meroney, R. N., Bouwmeester, (1981), "An Algorithm to Estimate Field Concentrations Under Nonsteady Meteorological Conditions from Wind Tunnel Experiments," Jornal of Applied Meteorology, Vol. 30, pp. 92-101.

Kothari, K. M., Meroney, R. N. and Peterka, J. A. (1979), "Nuclear Power Plant Building Works Effects on Atmosphere Diffusion," EPRI Report No. 1891, CER79-80KMK-RNM-JAP28, 109 pp.

Lamb, R. G. (1982), "Diffusion in the Convective Boundary Layer," Chapter 5, Atmospheric Turbulence and Air Pollution Modeling, Nieuwstadt and van Dop, editors, D. Reidel Publishing Company, Dordrecht, Holland, pp. 159-230.

Meroney, R. N. (1980), "Wind-Tunnel Simulations of the Flow Over Hills and Complex Terrain," J. of Industrial Aerodynamics, Vol. 5, pp. 297-321.

Meroney, R. N. (1982), "Turbulent Diffusion Near Buildings," Engineering Meteorology, Chapter 11, pp. 481-521.

Meroney, R. N., Cermak, J. E., and Garrison, J. A. (1975a), "Wind-Tunnel Study of Stack Gas Dispersal at Lansing Power Station, Units 1, 2, 3, and 4," FDDL Report No. CER74-75RNM-JEC-JAG28, Colorado State University, Fort Collins, Colorado.

Meroney, R. N., Cermak, J. E., and Garrison, J. A. (1975b), "Wind-Tunnel Study of Stack Gas Dispersal at Lansing Power Station, Units 1, 2, 3, and 4," FDDL Report No. CER74-75RNM-JEC-JAG29, Colorado State University, Fort Collins, Colorado.

Meroney, R. N., Sandborn, V. A., Bouwmeester, R. J. B., Chien, H. C., and Rider, M. (1978), "Sites for Wind-Power Installations: Physical Modeling of the Influence of Hills, Ridges and Complex Terrain - Part II: Executive Summary," Dept. of Energy Report RLO/2438-77/3, 90 pp.

Niemann, H. J. and Ruhwedel, J. (1980), "Full-scale and Model Tests on Wind-induced, Static and Dynamic Stresses in Cooling Tower Shells," Eng. Struct., Vol. 2, pp. 81-89.

Ogawa, Y., Diosey, P. G., Uehara, K., and Ueda, H. (1985), "Wind Tunnel Observation of Flow and Diffusion Under Stable Stratification," Atmos. Envir., Vol. 19, pp. 65-74.

Peterka, J. A., Meroney, R. N. and Kothari, K. (1985), "Wind Flow Patterns About Buildings," J. of Wind Engineering and Industrial Aerodynamics, Vol. 21, pp. 21-38.

Plate, E. J. and Cermak, J. E. (1963), "Micro-meteorological Wind-Tunnel Facility," Fluid Dynamics and Diffusion Laboratory Report CER63EJP-JEC9, Colorado State University, Fort Collins, Colorado, 65 pp.

Poreh, M. and Cermak, J. E. (1984), "Wind Tunnel Research on the Mechanics of Plumes in the Atmospheric Surface Layer, Part II," Annual Report to U.S. Dept. of Army, Chemical Systems Laboratory, Aberdeen Proving Ground, Maryland, Colorado State University Civil Engineering Department Report CER84-85MP-JEC47, 45 pp.

Fanga Raju, K. G. and Singh, V. (1976), "Blockage Effects on Drag of Sharp Edged Bodies," J. of Industrial Aerodynamics, Vol. 1, pp. 301-309.

Schlichting, H. (1968), Boundary Layer Theory, McGraw-Hill Book Company, New York, 774 pp.

Schon, J. P. and Mery, P. (1971), "A Preliminary Study of the Simulation of Neutral Atmospheric Boundary Layer Using Air Injection in a Wind Tunnel," Atmos. Enviro., Vol. 5, No. 5, pp. 299-312.

Sethurama, S., and Cermak, J. E. (1973), "Stratified Shear Flows Over a Simulated Three-Dimensional Urban Heat Island," Project Themis Technical Report No. 23, CER73-74SS-JEC4, Colorado State University, Fort Collins, Colorado.

Snyder, W. H., Britter, R. E., and Hunt, J. C. R. (1979), "A Fluid Modeling Study of the Flow Structure and Plume Impingement on a Three-Dimensional Hil in Stably Stratified Flow," Proc. Fifth Int. Conf. on Wind Engr., Pergamon Press, NY, Vol. 1, pp. 319-329.

Snyder, W. H. (1981), "Guidelines for Fluid Modeling of Atmospheric Diffusion," EPA Report EPA-600/8-81-009, 185 pp.

Szechenyi, E. (1975), "Supercritical Reynolds Number Simulation for Two dimensional Flow over Circular Cylinders," J. Fluid Mech., Vol. 70, pp. 529-542.

Teunissen, H. W. (1975), "Simulation of the Planetary Boundary Layer in a Multiple Jet Wind Tunnel," Atmos. Envir., Vol. 9, pp. 145-174.

Willis, G. E. and Deardorff, J. W. (1974), "A Laboratory Model of the Unstable Planetary Boundary Layer," J. Atmos. Sci., Vol. 31, pp. 1297-1307.

Willis, G. E. and Deardorff, J. W. (1976), "A Laboratory Model of Diffusion into the Convective Planetary Boundary Layer," Quart. J. Roy. Meteorol. Soc., Vol. 102, pp. 427-445.

Willis, G. E. and Deardorff, J. W. (1978), "A Laboratory Study of Dispersion from an Elevated Source Within a Modeled Convective Planetary Boundary Layer," Atmos. Envir., Vol. 12, pp. 1305-1311.

Yamada, T. and Meroney, R. N. (1971). "Numerical and Wind-Tunnel Simulation of Response of Stratified Shear Layers to Nonhomogeneous Surface Features," CER7071TY-RNM62, Colorado State University, also (AD-730-953).

TABLES

Table 1 Velocity Profile Conditions

Profile #	X Position	Y Position	Model Wind Direction (from N)	Reference Velocity (m/s)
1	Upwind	Tunnel Center	180	1.73
2	Upwind	+ 2 feet	180	1.73
3	Upwind	- 2 feet	180	1.73
4	Upwind	Tunnel Center	0	1.73
5	Upwind	Tunnel Center	0	3.45
6	Upwind	Tunnel Center	0	5.17
7	Model Center	Model Center	0	3.45
8	Model Center	Model Center	45	3.45
9	Model Center	Model Center	90	3.45
10	Model Center	Model Center	135	3.45
11	Model Center	Model Center	180	3.45
12	Model Center	Model Center	225	3.45
13	Model Center	Model Center	270	3.45
14	Model Center	Model Center	315	3.45

note: Model values for distance and velocity are used here.

Table 2 Velocity Profile Data for Profiles 1, 2 and 3

Normalized Height	--- Profile: No.1 --- Normalized Velocity	Turbulent Intensity (%)	--- Profile: No.2 --- Normalized Velocity	Turbulent Intensity (%)	--- Profile: No.3 --- Normalized Velocity	Turbulent Intensity (%)
0.026	0.292	37.7	0.320	37.2	0.281	42.0
0.033	0.317	35.8	0.355	35.1	0.348	38.7
0.043	0.405	31.9	0.419	28.1	0.398	30.8
0.053	0.427	27.9	0.449	28.9	0.455	31.6
0.064	0.472	26.6	0.487	26.5	0.523	27.6
0.083	0.528	27.1	0.551	24.3	0.559	22.9
0.103	0.582	20.9	0.598	21.0	0.651	19.3
0.128	0.614	20.4	0.640	21.3	0.655	18.7
0.154	0.642	18.3	0.662	19.0	0.727	16.3
0.177	0.736	14.2	0.726	16.0	0.750	15.9
0.203	0.725	13.7	0.738	14.8	0.751	14.9
0.253	0.758	13.4	0.806	11.9	0.806	11.4
0.300	0.823	10.2	0.843	10.3	0.830	10.5
0.400	0.857	9.6	0.869	8.0	0.876	7.9
0.500	0.901	8.2	0.902	8.0	0.898	7.4
0.600	0.910	7.0	0.928	6.9	0.929	6.3
0.800	0.946	5.4	0.967	6.0	0.973	5.2
1.000	0.998	5.4	0.999	5.6	1.002	5.4
1.200	1.036	6.3	1.035	5.8	1.073	6.2

Reference Height = 1260 ft.

Table 3 Velocity Profile Data for Profiles 4, 5 and 6

Normalized Height	--- Profile: No.4 --- Normalized Velocity	Turbulent Intensity (%)	--- Profile: No.5 --- Normalized Velocity	Turbulent Intensity (%)	--- Profile: No.6 --- Normalized Velocity	Turbulent Intensity (%)
0.026	0.299	41.8	0.295	43.5	0.323	38.1
0.033	0.371	33.0	0.361	33.8	0.378	32.4
0.043	0.435	28.2	0.417	28.9	0.460	28.0
0.053	0.486	26.0	0.475	25.5	0.484	26.2
0.064	0.495	25.6	0.484	25.1	0.510	24.8
0.083	0.563	22.2	0.555	23.2	0.576	20.7
0.103	0.637	18.5	0.624	20.4	0.618	18.2
0.128	0.678	17.0	0.668	19.5	0.652	17.6
0.154	0.704	15.8	0.689	16.1	0.681	16.4
0.177	0.730	14.6	0.735	15.4	0.714	14.7
0.203	0.752	14.1	0.759	13.7	0.743	12.8
0.253	0.781	12.2	0.813	13.7	0.780	12.0
0.300	0.810	10.2	0.851	10.3	0.820	10.3
0.400	0.867	8.9	0.890	7.9	0.853	8.0
0.500	0.902	10.0	0.900	7.0	0.890	7.1
0.600	0.933	6.1	0.935	6.4	0.924	6.3
0.800	0.957	5.9	0.978	5.3	0.955	5.3
1.000	1.000	5.5	0.998	5.3	1.000	5.6
1.200	1.066	5.6	1.056	5.7	1.048	5.8

Reference Height = 1260 ft.

Table 4 Velocity Profile Data for Profiles 7, 8, 9 and 10

Normalized Height	-- Profile: No.7 --- Normalized Velocity	Turbulent Intensity (%)	-- Profile: No.8 --- Normalized Velocity	Turbulent Intensity (%)	-- Profile: No.9 --- Normalized Velocity	Turbulent Intensity (%)	-- Profile: No.10 -- Normalized Velocity	Turbulent Intensity (%)
0.026	0.286	27.6	0.252	40.2	0.281	47.1	0.239	37.9
0.033	0.297	28.3	0.250	39.8	0.306	43.2	0.242	39.5
0.043	0.318	29.0	0.304	38.9	0.342	40.1	0.296	38.4
0.053	0.351	29.7	0.348	39.0	0.453	31.1	0.341	32.5
0.064	0.358	28.7	0.383	35.1	0.505	26.9	0.371	30.7
0.083	0.419	29.4	0.463	28.4	0.541	23.5	0.414	25.6
0.103	0.462	28.2	0.494	26.5	0.591	19.4	0.460	24.6
0.128	0.539	25.3	0.588	22.7	0.618	18.8	0.486	23.2
0.154	0.558	22.6	0.602	21.7	0.662	16.5	0.546	21.2
0.177	0.611	19.7	0.650	19.0	0.672	16.0	0.577	19.0
0.203	0.669	17.8	0.674	17.8	0.684	15.5	0.626	17.7
0.253	0.719	15.3	0.718	14.6	0.753	12.8	0.696	14.8
0.300	0.757	12.8	0.772	12.8	0.790	12.0	0.733	15.0
0.400	0.823	9.9	0.829	10.5	0.835	9.3	0.854	11.7
0.500	0.860	8.4	0.894	8.1	0.893	7.7	0.915	7.5
0.600	0.910	6.9	0.921	7.4	0.910	7.0	0.941	6.1
0.800	0.944	5.6	0.983	5.2	0.970	5.2	0.974	5.4
1.000	1.000	5.1	1.000	5.2	0.999	5.0	1.000	4.7
1.200	1.048	5.7	1.054	5.6	1.024	5.3	1.032	5.2

Reference Height = 1260 ft.

Table 5 Velocity Profile Data for Profiles 11, 12, 13 and 14

Normalized Height	-- Profile: No.11 -- Normalized Velocity	Turbulent Intensity (%)	-- Profile: No.12 -- Normalized Velocity	Turbulent Intensity (%)	-- Profile: No.13 -- Normalized Velocity	Turbulent Intensity (%)	-- Profile: No.14 -- Normalized Velocity	Turbulent Intensity (%)
0.026	0.239	37.9	0.155	42.0	0.238	45.7	0.208	29.0
0.033	0.242	39.5	0.153	42.2	0.248	42.7	0.216	30.0
0.043	0.296	38.4	0.161	41.8	0.319	40.9	0.237	31.2
0.053	0.341	32.5	0.165	41.1	0.386	34.5	0.264	32.7
0.064	0.371	30.7	0.183	36.8	0.441	31.1	0.305	33.7
0.083	0.414	25.6	0.190	42.9	0.526	25.9	0.393	32.1
0.103	0.460	24.6	0.199	43.8	0.619	20.6	0.490	28.3
0.128	0.486	23.2	0.217	42.4	0.666	18.2	0.544	23.2
0.154	0.546	21.2	0.247	43.2	0.710	15.5	0.642	19.0
0.177	0.577	19.0	0.264	42.5	0.715	15.1	0.674	19.6
0.203	0.626	17.7	0.301	40.0	0.758	13.1	0.696	16.3
0.253	0.696	14.8	0.412	33.4	0.800	12.2	0.770	13.2
0.300	0.733	15.0	0.476	28.5	0.817	11.3	0.818	11.6
0.400	0.854	11.7	0.649	23.1	0.891	9.0	0.869	10.2
0.500	0.915	7.5	0.811	16.9	0.917	6.8	0.904	7.1
0.600	0.941	6.1	0.931	9.2	0.927	5.8	0.934	6.2
0.800	0.974	5.4	0.980	5.1	0.973	5.5	0.972	4.8
1.000	1.000	4.7	1.001	4.5	0.999	4.8	1.001	4.8
1.200	1.032	5.2	1.026	4.8	1.028	5.2	1.046	5.5

Reference Height = 1260 ft.

Table 6 Visualization Test Conditions

Run No.	Building Height $(ft)_p$	Garage Height $(ft)_p$	Stack Height $(ft)_p$	Exit Velocity $(fpm)_p$	Wind Dir. (from)	Camera Position
1	75	42	100	800	N	1
2	75	42	100	1600	N	1
3	75	42	100	3200	N	1
4	75	42	100	800	NNE	1
5	75	42	100	1600	NNE	1
6	75	42	100	3200	NNE	1
7	75	42	100	800	ENE	1
8	75	42	100	1600	ENE	1
9	75	42	100	3200	ENE	1
10	75	42	100	800	SE	3
11	75	42	100	1600	SE	3
12	75	42	100	3200	SE	3
13	75	42	100	800	SSW	3
14	75	42	100	1600	SSW	3
15	75	42	100	3200	SSW	3
16	75	42	100	800	SW	3
17	75	42	100	1600	SW	3
18	75	42	100	3200	SW	3
19	75	42	100	800	WSW	3
20	75	42	100	1600	WSW	3
21	75	42	100	3200	WSW	3
22	75	42	100	800	NW	5
23	75	42	100	1600	NW	5
24	75	42	100	3200	NW	5
25	75	75	100	800	NNE	1
26	75	75	100	1600	NNE	1
27	75	75	100	3200	NNE	1
28	75	75	100	800	ENE	1
29	75	75	100	1600	ENE	1
30	75	75	100	3200	ENE	1
31	75	75	100	800	SE	3
32	75	75	100	1600	SE	3
33	75	75	100	3200	SE	3
34	75	75	100	800	NW	5
35	75	75	100	1600	NW	5
36	75	75	100	3200	NW	5
37	53	42	100	800	N	1
38	53	42	100	1600	N	1
39	53	42	100	3200	N	1
40	53	42	100	800	NNE	1
41	53	42	100	1600	NNE	1
42	53	42	100	3200	NNE	1
43	53	42	100	800	ENE	1
44	53	42	100	1600	ENE	1
45	53	42	100	3200	ENE	1
46	53	42	100	800	SE	3
47	53	42	100	1600	SE	3
48	53	42	100	3200	SE	3
49	53	42	100	800	SSW	3
50	53	42	100	1600	SSW	3

Table 7 Visualization Test Conditions (continued)

Run No.	Building Height $(ft)_p$	Garage Height $(ft)_p$	Stack Height $(ft)_p$	Exit Velocity $(fpm)_p$	Wind Dir. (from)	Camera Position
51	53	42	100	3200	SSW	3
52	53	42	100	800	SW	3
53	53	42	100	1600	SW	3
54	53	42	100	3200	SW	3
55	53	42	100	800	WSW	3
56	53	42	100	1600	WSW	3
57	53	42	100	3200	WSW	3
58	53	42	100	800	NW	5
59	53	42	100	1600	NW	5
60	53	42	100	3200	NW	5
61	75	42	125	1600	NNE	1
62	75	42	125	1600	ENE	1
63	75	42	125	1600	SE	3
64	75	42	125	1600	NW	5
65	75	75	125	800	N	1
66	75	75	125	1600	N	1
67	75	75	125	3200	N	1
68	75	75	125	800	NNE	1
69	75	75	125	1600	NNE	1
70	75	75	125	3200	NNE	1
71	75	75	125	800	ENE	1
72	75	75	125	1600	ENE	1
73	75	75	125	3200	ENE	1
74	75	75	125	800	SE	3
75	75	75	125	1600	SE	3
76	75	75	125	3200	SE	3
77	75	75	125	800	SSW	3
78	75	75	125	1600	SSW	3
79	75	75	125	3200	SSW	3
80	75	75	125	800	SW	3
81	75	75	125	1600	SW	3
82	75	75	125	3200	SW	3
83	75	75	125	800	WSW	3
84	75	75	125	1600	WSW	3
85	75	75	125	3200	WSW	3
86	75	75	125	800	NW	5
87	75	75	125	1600	NW	5
88	75	75	125	3200	NW	5
89	90	90	125	800	NNE	1
90	90	90	125	1600	NNE	1
91	90	90	125	3200	NNE	1
92	90	90	125	800	ENE	1
93	90	90	125	1600	ENE	1
94	90	90	125	3200	ENE	1
95	90	90	125	800	SE	3
96	90	90	125	1600	SE	3
97	90	90	125	3200	SE	3
98	90	90	125	800	NW	5
99	90	90	125	1600	NW	5
100	90	90	125	3200	NW	5

Table 8 Visualization Test Conditions (continued)

Run No.	Building Height $(ft)_p$	Garage Height $(ft)_p$	Stack Height $(ft)_p$	Exit Velocity $(fpm)_p$	Wind Dir. (from)	Camera Position
101	75	42	150	1600	NNE	1
102	75	42	150	1600	ENE	1
103	75	42	150	1600	SE	3
104	75	42	150	1600	NW	5
105	75	75	150	800	N	1
106	75	75	150	1600	N	1
107	75	75	150	3200	N	1
108	75	75	150	800	NNE	1
109	75	75	150	1600	NNE	1
110	75	75	150	3200	NNE	1
111	75	75	150	800	ENE	1
112	75	75	150	1600	ENE	1
113	75	75	150	3200	ENE	1
114	75	75	150	800	SE	3
115	75	75	150	1600	SE	3
116	75	75	150	3200	SE	3
117	75	75	150	800	SSW	3
118	75	75	150	1600	SSW	3
119	75	75	150	3200	SSW	3
120	75	75	150	800	SW	3
121	75	75	150	1600	SW	3
122	75	75	150	3200	SW	3
123	75	75	150	800	WSW	3
124	75	75	150	1600	WSW	3
125	75	75	150	3200	WSW	3
126	75	75	150	800	NW	5
127	75	75	150	1600	NW	5
128	75	75	150	3200	NW	5
129	90	90	150	800	NNE	1
130	90	90	150	1600	NNE	1
131	90	90	150	3200	NNE	1
132	90	90	150	800	ENE	1
133	90	90	150	1600	ENE	1
134	90	90	150	3200	ENE	1
135	90	90	150	800	SE	1
136	90	90	150	1600	SE	1
137	90	90	150	3200	SE	1
138	90	90	150	800	NW	5
139	90	90	150	1600	NW	5
140	90	90	150	3200	NW	5
141	90	90	225	800	NNE	1
142	90	90	225	1600	NNE	1
143	90	90	225	3200	NNE	1
144	90	90	225	800	ENE	1
145	90	90	225	1600	ENE	1
146	90	90	225	3200	ENE	1
147	90	90	225	800	SE	3
148	90	90	225	1600	SE	3
149	90	90	225	3200	SE	3
150	90	90	225	800	SSW	3

Table 9 Visualization Test Conditions (continued)

Run No.	Building Height $(ft)_p$	Garage Height $(ft)_p$	Stack Height $(ft)_p$	Exit Velocity $(fpm)_p$	Wind Dir. (from)	Camera Position
151	90	90	225	1600	SSW	3
152	90	90	225	3200	SSW	3
153	90	90	225	800	WSW	3
154	90	90	225	1600	WSW	3
155	90	90	225	3200	WSW	3
156	90	90	225	800	NW	5
157	90	90	225	1600	NW	5
158	90	90	225	3200	NW	5
159	375	42	400	800	NNE	1
160	375	42	400	1600	NNE	1
161	375	42	400	800	ENE	1
162	375	42	400	1600	ENE	1
163	375	42	400	800	SE	3
164	375	42	400	1600	SE	3
165	375	42	400	800	WSW	3
166	375	42	400	1600	WSW	3
167	375	42	400	800	NW	5
168	375	42	400	1600	NW	5
169	0	0	100	1600	SE	3
170	0	0	100	1600	SSW	3
171	0	0	100	1600	WSW	3
172	0	0	100	1600	NW	5
173	0	0	125	1600	SE	3
174	0	0	125	1600	SSW	3
175	0	0	125	1600	WSW	3
176	0	0	125	1600	NW	5
177	0	0	150	1600	SE	3
178	0	0	150	1600	SSW	3
179	0	0	150	1600	WSW	3
180	0	0	150	1600	NW	5
181	0	0	225	1600	SE	3
182	0	0	225	1600	SSW	3
183	0	0	225	1600	WSW	3
184	0	0	225	1600	NW	5
185	0	0	400	1600	SE	3
186	0	0	400	1600	SSW	3
187	0	0	400	1600	WSW	3
188	0	0	400	1600	NW	5
189	75	75	150	1600	NNW	5
190	100	-	200	800	N	5
191	100	-	200	1600	N	5
192	100	-	200	800	NNE	5
193	100	-	200	1600	NNE	5
194	100	-	200	800	NW	6
195	100	-	200	1600	NW	6
196	100	-	200	800	NNW	6
197	100	-	200	1600	NNW	6

Table 10 Visual Test Results Summary

Run No.	Bldg Height (ft)	Stack Height (ft)	Exit Velocity (fpm)	Wind Dir (from)	Observed Plume Behavior: Stack Downwash	Building Downwash	Cavity Mixing	Plume Descent	Plume Lofting	Skyscraper Impingment
1	75	100	800	N	X			X		X
2	75	100	1600	N					X	X
3	75	100	3200	N					X	X
4	75	100	800	NNE	X			X		
5	75	100	1600	NNE					X	
6	75	100	3200	NNE					X	
7	75	100	800	ENE	X	X		X		
8	75	100	1600	ENE	X			X		
9	75	100	3200	ENE					X	
10	75	100	800	SE	X			X		
11	75	100	1600	SE					X	
12	75	100	3200	SE					X	
13	75	100	800	SSW	X	X	X	X		
14	75	100	1600	SSW	X	X	X	X		
15	75	100	3200	SSW	X	X	X			
16	75	100	800	SW	X	X	X	X		
17	75	100	1600	SW	X	X		X		
18	75	100	3200	SW					X	
19	75	100	800	WSW	X	X	X	X		
20	75	100	1600	WSW	X	X	X	X		
21	75	100	3200	WSW	X	X	X		X	
22	75	100	800	NW	X				X	
23	75	100	1600	NW					X	
24	75	100	3200	NW					X	
25	75	100	800	NNE				X		
26	75	100	1600	NNE					X	
27	75	100	3200	NNE					X	
28	75	100	800	ENE	X			X		
29	75	100	1600	ENE	X				X	
30	75	100	3200	ENE					X	
31	75	100	800	SE	X				X	
32	75	100	1600	SE					X	
33	75	100	3200	SE					X	
34	75	100	800	NW	X			X		
35	75	100	1600	NW	X					
36	75	100	3200	NW					X	
37	53	100	800	N	X	X		X		X
38	53	100	1600	N	X				X	X
39	53	100	3200	N					X	X
40	53	100	800	NNE	X	X		X		X
41	53	100	1600	NNE	X				X	X
42	53	100	3200	NNE					X	X
43	53	100	800	ENE	X			X		
44	53	100	1600	ENE	X			X		
45	53	100	3200	ENE					X	
46	53	100	800	SE	X			X		
47	53	100	1600	SE				X		
48	53	100	3200	SE					X	
49	53	100	800	SSW	X	X	X	X		
50	53	100	1600	SSW	X	X	X	X		
51	53	100	3200	SSW	X					
52	53	100	800	SW	X	X	X	X		
53	53	100	1600	SW	X	X	X	X		
54	53	100	3200	SW					X	
55	53	100	800	WSW	X	X	X	X		
56	53	100	1600	WSW	X	X	X	X		
57	53	100	3200	WSW	X	X	X	X		
58	53	100	800	NW	X			X		
59	53	100	1600	NW	X				X	
60	53	100	3200	NW					X	
61	75	125	1600	NNE	X				X	X
62	75	125	1600	ENE	X				X	
63	75	125	1600	SE	X				X	
64	75	125	1600	NW	X				X	
65	75	125	800	N	X	X		X		X

Table 11 Visual Test Results Summary (continued)

Run No.	Bldg Height (ft)	Stack Height (ft)	Exit Velocity (fpm)	Wind Dir (from)	Observed Plume Behavior: Stack Downwash	Building Downwash	Cavity Mixing	Plume Descent	Plume Lofting	Skyscraper Impingment
66	75	125	1600	N	X			X		X
67	75	125	3200	N					X	X
68	75	125	800	NNE	X	X		X		X
69	75	125	1600	NNE	X				X	X
70	75	125	3200	NNE	X				X	X
71	75	125	800	ENE	X	X	X	X		
72	75	125	1600	ENE	X					
73	75	125	3200	ENE					X	
74	75	125	800	SE	X	X		X		
75	75	125	1600	SE	X				X	
76	75	125	3200	SE					X	
77	75	125	800	SSW	X	X	X	X		
78	75	125	1600	SSW	X	X			X	
79	75	125	3200	SSW	X				X	
80	75	125	800	SW	X	X	X	X		
81	75	125	1600	SW	X	X		X		
82	75	125	3200	SW					X	
83	75	125	800	WSW	X	X	X	X		
84	75	125	1600	WSW	X	X	X	X		
85	75	125	3200	WSW	X	X				
86	75	125	800	NW	X			X		
87	75	125	1600	NW	X				X	
88	75	125	3200	NW					X	
89	90	125	800	NNE	X			X		X
90	90	125	1600	NNE					X	X
91	90	125	3200	NNE					X	X
92	90	125	800	ENE	X	X		X		
93	90	125	1600	ENE	X					
94	90	125	3200	ENE	X				X	
95	90	125	800	SE	X	X		X		
96	90	150	1600	SE	X				X	
97	90	150	3200	SE					X	
98	90	150	800	NW	X	X		X		
99	90	150	1600	NW	X				X	
100	90	150	3200	NW					X	
101	75	150	1600	NNE	X				X	X
102	75	150	1600	ENE	X			X		
103	75	150	1600	SE	X				X	
104	75	150	1600	NW	X				X	
105	75	150	800	N	X	X		X		X
106	75	150	1600	N	X				X	X
107	75	150	3200	N					X	X
108	75	150	800	NNE	X	X		X		X
109	75	150	1600	NNE	X				X	X
110	75	150	3200	NNE					X	X
111	75	150	800	ENE	X	X		X		
112	75	150	1600	ENE	X				X	
113	75	150	3200	ENE					X	
114	75	150	800	SE	X	X		X		
115	75	150	1600	SE	X				X	
116	75	150	3200	SE					X	
117	75	150	800	SSW	X	X	X	X		
118	75	150	1600	SSW	X	X	X		X	
119	75	150	3200	SSW	X				X	
120	75	150	800	SW	X	X	X	X		
121	75	150	1600	SW	X	X				
122	75	150	3200	SW	X				X	
123	75	150	800	WSW	X	X	X	X		
124	75	150	1600	WSW	X	X	X	X		
125	75	150	3200	WSW	X	X			X	
126	75	150	800	NW	X	X		X		
127	75	150	1600	NW	X				X	
128	75	150	3200	NW					X	
129	90	150	800	NNE	X			X		X
130	90	150	1600	NNE	X				X	X

Table 12 Visual Test Results Summary (continued)

Run No.	Bldg Height (ft)	Stack Height (ft)	Exit Velocity (fpm)	Wind Dir (from)	Observed Plume Behavior: Stack Downwash	Building Downwash	Cavity Mixing	Plume Descent	Plume Lofting	Skyscraper Impingment
131	90	150	3200	NNE					X	X
132	90	150	800	ENE	X	X		X		
133	90	150	1600	ENE	X				X	
134	90	150	3200	ENE					X	
135	90	150	800	SE	X			X		
136	90	150	1600	SE					X	
137	90	150	3200	SE					X	
138	90	150	800	NW	X			X		
139	90	150	1600	NW	X				X	
140	90	150	3200	NW					X	
141	90	225	800	NNE	X			X		X
142	90	225	1600	NNE					X	X
143	90	225	3200	NNE					X	X
144	90	225	800	ENE	X			X		
145	90	225	1600	ENE					X	
146	90	225	3200	ENE					X	
147	90	225	800	SE	X			X		
148	90	225	1600	SE					X	
149	90	225	3200	SE					X	
150	90	225	800	SSW	X	X				
151	90	225	1600	SSW	X	X			X	
152	90	225	3200	SSW					X	
153	90	225	800	WSW	X	X	X	X		
154	90	225	1600	WSW	X	X	X	X		
155	90	225	3200	WSW	X				X	
156	90	225	800	NW	X				X	
157	90	225	1600	NW					X	
158	90	225	3200	NW					X	
159	375	400	800	NNE	X				X	X
160	375	400	1600	NNE					X	X
161	375	400	800	ENE					X	
162	375	400	1600	ENE					X	
163	375	400	800	SE					X	
164	375	400	1600	SE					X	
165	375	400	800	WSW	X	X		X		
166	375	400	1600	WSW	X	X		X		
167	375	400	800	NW	X				X	
168	375	400	1600	NW	X				X	
189	75	150	1600	NNW	X				X	X
190	100	200	800	N	X			X		X
191	100	200	1600	N						X
192	100	200	800	NNE	X			X		X
193	100	200	1600	NNE					X	X
194	100	200	800	NW					X	
195	100	200	1600	NW					X	
196	100	200	800	NNW					X	X
197	100	200	1600	NNW					X	X

Table 13 Concentration Sampling Locations

Point No.	Code No.	Description	Field Distance (ft)	Field Direction (degrees)	Field Elevation (ft)	Model Distance (cm)	Model Elevation (cm)
1	S1	N 600m Downwind	1968	0	0	156.2	0.0
2	A2	St. Mary's School	765	8	0	60.7	0.0
3	A8	Basketball Court	602	22	0	47.8	0.0
4	A6	C.C. Youth Center	1078	33	19	85.6	1.5
5	R4	Existing Road	342	36	55	27.2	4.4
6	S2	NE 600m Downwind	1968	45	0	156.2	0.0
7	A9	Prince St.	1219	46	0	96.8	0.0
8	A5	Hanover St.	899	48	0	71.4	0.0
9	A1	Blackstone St.	102	53	0	8.1	0.0
10	A4	Boston Police Acad.	749	62	0	59.4	0.0
11	S9	ENE 600m Downwind	1968	67	0	156.2	0.0
12	A10	Callahan Tunnel Bldg	1165	67	54	92.5	4.3
13	A11	Future Park	406	68	0	32.3	0.0
14	A13	Commercial	1462	75	0	116.1	0.0
15	A12	North St.	848	78	0	67.3	0.0
16	E1	Commercial&Fulton	1152	83	0	91.4	0.0
17	B8	Play Area	1680	92	0	133.4	0.0
18	B10	Mercantile Mall	1187	103	0	94.2	0.0
19	B7	New England T&T	1750	118	0	138.9	0.0
20	B1	Marshall St.	102	122	0	8.1	0.0
21	R3	Hanover St. Bldg	163	123	36	13.0	2.8
22	B6	Parking Garage	634	123	0	50.3	0.0
23	E2	South Market St.	912	126	0	72.4	0.0
24	R9	Creek Square Bldg	506	132	74	40.1	5.8
25	B5	State St. Bldg	1203	153	0	95.5	0.0
26	B4	Faneuil Flower Mkt.	691	155	0	54.9	0.0
27	R2	Hanover St. Bldg	173	157	55	13.7	4.4
28	B2	Congress St. Bldg	890	169	0	70.6	0.0
29	B3	Congress St.	1421	172	0	112.8	0.0
30	B9	Union St.	173	178	0	13.7	0.0
31	R1	Boston City Hall	522	191	120	41.4	9.5
32	R1A	Boston City Hall	915	199	0	72.6	0.0
33	R5	Fed. Bldg. Plaza	326	227	0	25.9	0.0
34	C1	Pool	832	230	0	66.0	0.0
35	C2	New Fed. Bldg	301	236	0	23.9	0.0
36	R8	JFK Fed. Bldg	816	248	355	64.8	28.2
37	R6	New Fed. Bldg	314	254	69	24.9	5.5
38	D3	State Service Center	1376	289	0	109.2	0.0
39	D2	Portland St.	810	297	0	64.3	0.0
40	D8	Market St.	704	310	0	55.9	0.0
41	D9	Sudbury	282	315	0	22.4	0.0
42	D7	Canal & Causeway	1552	320	0	123.2	0.0
43	D1	Canal St.	752	320	0	59.7	0.0
44	R7	Gov. Center Garage	352	321	107	27.9	8.5
45	E3	New Boston Gardens	1701	321	0	135.0	0.0
46	E4	New Boston Gardens	1701	321	400	135.0	31.8
47	D6	Vent Bldg-Upper Intake	224	334	75	17.8	6.0
48	D5	Vent Bldg-Bottom Intake	224	335	0	17.8	0.0
49	D4	Washington	1069	344	0	84.8	0.0

Table 14 Concentration Test Conditions

Run No.	Vent Site	FIELD VALUES Building Height (ft)	Garage Height (ft)	Stack Height (ft)	Exit Velocity (fpm)	Intake Flow (cfs)	Wind Speed (mps)	Wind Dir. (from)	MODEL VALUES Wind Speed (cm/s)	Exhaust Flow (ccs)	Intake Flow (ccs)
1	Parcel 7	75	75	100	1600	34,468	5.0	WSW	50	1000	660
2	Parcel 7	75	75	100	1600	34,468	5.0	SE	50	1000	660
3	Parcel 7	75	75	125	1600	34,468	5.0	WSW	50	1000	660
4	Parcel 7	75	75	125	1600	34,468	5.0	SE	50	1000	660
5	Parcel 7	75	75	150	800	17,234	5.0	WSW	50	500	330
6	Parcel 7	75	75	150	800	17,234	5.0	SE	50	500	330
7	Parcel 7	75	75	150	1600	34,468	5.0	WSW	50	1000	660
8	Parcel 7	75	75	150	1600	34,468	5.0	SE	50	1000	660
9	Parcel 7	75	75	150	3200	68,935	5.0	WSW	50	2000	1320
10	Parcel 7	75	75	150	3200	68,935	5.0	SE	50	2000	1320
11	Parcel 7	90	90	225	1600	34,468	5.0	WSW	50	1000	660
12	Parcel 7	90	90	225	1600	34,468	5.0	SE	50	1000	660
13	Parcel 7	75	75	150	1600	34,468	5.0	ENE	50	1000	660
14	Parcel 7	75	75	150	1600	34,468	5.0	NNE	50	1000	660
15	Parcel 7	75	75	150	400	0	2.5	WSW	25	250	0
16	Parcel 7	75	75	150	800	0	5.0	WSW	50	500	0
17	Parcel 7	75	75	150	1200	0	7.5	WSW	75	750	0
18	Parcel 7	75	75	150	1600	0	10.0	WSW	100	1000	0
19	Parcel 7	75	75	150	2000	0	12.5	WSW	125	1250	0
20	Parcel 7	75	75	150	800	0	5.0	S	50	500	0
21	Parcel 7	75	75	150	1200	0	7.5	S	75	750	0
22	Parcel 7	75	75	150	1600	0	10.0	S	100	1000	0
23	Parcel 7	75	75	150	800	0	5.0	NNE	50	500	0
24	Parcel 7	75	75	150	1200	0	7.5	NNE	75	750	0
25	Parcel 7	75	75	150	1600	0	10.0	NNE	100	1000	0
26	Parcel 7	75	75	125	1600	34,468	5.0	N	50	1000	660
27	Parcel 7	75	75	125	1600	34,468	5.0	NE	50	1000	660
28	Parcel 7	75	75	125	1600	34,468	5.0	E	50	1000	660
29	Parcel 7	75	75	125	1600	34,468	5.0	ESE	50	1000	660
30	Parcel 7	75	75	125	1600	34,468	5.0	SSE	50	1000	660
31	Parcel 7	75	75	125	1600	34,468	5.0	S	50	1000	660
32	Parcel 7	75	75	125	1600	34,468	5.0	SSW	50	1000	660
33	Parcel 7	75	75	125	1600	34,468	5.0	SW	50	1000	660
34	Parcel 7	75	75	125	1600	34,468	5.0	W	50	1000	660
35	Parcel 7	75	75	125	1600	34,468	5.0	WNW	50	1000	660
36	Parcel 7	75	75	125	1600	34,468	5.0	NNW	50	1000	660
37	Parcel 7	75	75	125	800	17,234	5.0	NNE	50	500	330
38	Parcel 7	75	75	125	1600	34,468	5.0	NNE	50	1000	660
39	Parcel 7	75	75	125	3200	68,935	5.0	NNE	50	2000	1320
40	Parcel 7	75	75	125	800	17,234	5.0	ENE	50	500	330
41	Parcel 7	75	75	125	1600	34,468	5.0	ENE	50	1000	660
42	Parcel 7	75	75	125	3200	68,935	5.0	ENE	50	2000	1320
43	Parcel 7	75	75	125	400	8,617	5.0	WSW	50	500	165
44	Parcel 7	75	75	125	800	17,234	5.0	WSW	50	1000	330
45	Parcel 7	75	75	125	3200	68,935	5.0	WSW	50	2000	1320
46	Parcel 7	75	75	125	400	8,617	5.0	SE	50	500	165
47	Parcel 7	75	75	125	800	17,234	5.0	SE	50	1000	330
48	Parcel 7	75	75	125	3200	68,935	5.0	SE	50	2000	1320
49	Parcel 7	75	75	125	800	17,234	5.0	NW	50	500	330
50	Parcel 7	75	75	125	1600	34,468	5.0	NW	50	1000	660
51	Parcel 7	75	75	150	1600	34,468	5.0	ENE	50	1000	660
52	Parcel 7	75	75	150	1600	34,468	5.0	NNE	50	1000	660
53	Stack only	0	0	125	1600	34,468	5.0	NNE	50	1000	660
54	Stack only	0	0	125	1600	34,468	5.0	ENE	50	1000	660
55	Stack only	0	0	125	1600	34,468	5.0	SE	50	1000	660
56	Stack only	0	0	125	1600	34,468	5.0	WSW	50	1000	660
57	P7 no city	75	75	125	1600	34,468	5.0	N	50	1000	660
58	P7 no city	75	75	125	1600	34,468	5.0	E	50	1000	660
59	P7 no city	75	75	125	1600	34,468	5.0	SE	50	1000	660
60	P7 no city	75	75	125	1600	34,468	5.0	SW	50	1000	660
61	St Charles	100	-	200	400	8,617	5.0	NNW	50	250	165
62	St Charles	100	-	200	800	17,234	5.0	NNW	50	500	330
63	St Charles	100	-	200	1600	34,468	5.0	NNW	50	1000	660
64	St Charles	100	-	200	800	17,234	5.0	NW	50	500	330
65	St Charles	100	-	200	800	17,234	5.0	N	50	500	330
66	St Charles	100	-	200	800	17,234	5.0	NNE	50	500	330
67	St Charles	100	-	200	800	17,234	5.0	NE	50	500	330

Table 15 Concentration Results

Run no. =				1	2	3	4	5	6	7	8	9	10	11	12	13	14	15	16
Point No.	Description	X (ft)	Y (Deg)	Z (ft)	K^	K^	K^	K^	K^	K^	K^	K^	K^	K^	K^	K^	K^	K^	K^	K^
1	N 600m Downwind	1968	0	0																
2	St. Mary's School	765	8	0																
3	Basketball Court	602	22	0	0		0		0		0		0		0				1	0
4	C.C. Youth Center	1078	33	19	0		0		27		1		0		0				0	0
5	Existing Road	342	36	55	295		281		946		89		0		7				149	392
6	NE 600m Downwind	1968	45	0	0		3		20		4		1		0				1	4
7	Prince St.	1219	46	0	391		360		1044		221		53		46				42	626
8	Hanover St.	899	48	0	804		975		1827		457		81		100				250	1820
9	Blackstone St.	102	53	0	134		178		197		57		37		42				397	180
10	Boston Police Acad.	749	62	0	3401		3904		5703		2063		545		893				5361	8513
11	ENE 600m Downwind	1968	67	0	2102		2114		2493		1839		923		1605				527	2570
12	Callahan Tunnel Bldg	1165	67	54	4733		5354		5887		4072		1260		2574				3417	6406
13	Future Park	406	68	0	1615		2177		4453		948		75		138				1512	3226
14	Commercial	1462	75	0	4817		5259		6635		4756		2066		3569				5302	7336
15	North St.	848	78	0	5302		6311		9609		4551		1998		2538				7494	11248
16	Commercial&Fulton	1152	83	0																
17	Play Area	1680	92	0	2663		2951		4195		2318		811		1196				3061	4835
18	Mercantile Mall	1187	103	0	3670		3026		4666		2336		707		634				3005	4727
19	New England T&T	1750	118	0	299		631		305		469		48		188				1	380
20	Marshall St.	102	122	0	11		32		79		38		36		40			125	200	114
21	Hanover St. Bldg	163	123	36	144		53		145		24		11		34			6	451	155
22	Parking Garage	634	123	0	2297		1601		2450		1010		156		89			0	2618	2572
23	South Market St.	912	126	0																
24	Creek Square Bldg	506	132	74	17		36		53		24		2		1			0	33	29
25	State St. Bldg	1203	153	0														0		
26	Faneuil Flower Mkt.	691	155	0														0		
27	Hanover St. Bldg	173	157	55	0		11		29		13		8		27			1638	91	36
28	Congress St. Bldg	890	169	0														0		
29	Congress St.	1421	172	0														1		
30	Union St.	173	178	0													0	335		
31	Boston City Hall	522	191	120													0	1626		
32	Boston City Hall	915	199	0													0	313		
33	Fed. Bldg. Plaza	326	227	0													6	407		
34	Pool	832	230	0													516	73		
35	New Fed. Bldg	301	236	0													55	307		
36	JFK Fed. Bldg	816	248	355		1		58		0		0		0		0	7055	0		
37	New Fed. Bldg	314	254	69		1		0		1		1		0		3	869	1		
38	State Service Center	1376	289	0		712		928		1974		661		289		133	0	0		
39	Portland St.	810	297	0		1607		1741		5634		1950		529		338	0			
40	Market St.	704	310	0		2329		3340		5453		2075		361		286	0			
41	Sudbury	282	315	0		933		822		4136		523		53		46	43			
42	Canal & Causeway	1552	320	0		1055		1345		1967		1043		173		245				
43	Canal St.	752	320	0		1033		1537		2710		868		127		67				
44	Gov. Center Garage	352	321	107		1149		1945		3444		477		99		53				
45	New Boston Gardens	1701	321	0																
46	New Boston Gardens	1701	321	400																
47	Vent Bldg-Upper	224	334	75		500		524		1315		177		226		68				
48	Vent Bldg-Bottom	224	335	0		286		230		1343		168		26		21				
49	Washington	1069	344	0		2		1		3		1		0		0				

note $K^{\wedge} = (\chi U/Q)*10^{9}$ $[ft^{-2}]$

Table 16 Concentration Results (continued)

Run no. =				17	18	19	20	21	22	23	24	25	26	27	28	29	30	31	32
Point No.	Description	X (ft)	Y (Deg)	Z (ft)	K^	K^	K^	K^	K^	K^	K^	K^	K^	K^	K^	K^	K^	K^	K^	K^
1	N 600m Downwind	1968	0	0				2085	2252	2724								0	1961	36
2	St. Mary's School	765	8	0				995	1189	1643								0	1204	1076
3	Basketball Court	602	22	0	0	9	0	374	573	1291								0	675	2398
4	C.C. Youth Center	1078	33	19	0	11	0	3	19	76								0	98	3084
5	Existing Road	342	36	55	175	249	316	0	3	5								0	179	2451
6	NE 600m Downwind	1968	45	0	3	14	0	0	0	4								0	0	192
7	Prince St.	1219	46	0	575	363	431	0	0	3								0	0	638
8	Hanover St.	899	48	0	1900	1246	1452	0	0	3								0	5	1041
9	Blackstone St.	102	53	0	181	205	178	93	38	36				104				26	206	632
10	Boston Police Acad.	749	62	0	8780	9008	7832	3	4	0				17					35	259
11	ENE 600m Downwind	1968	67	0	2773	2468	2504	0	0	9				0					0	0
12	Callahan Tunnel Bldg	1165	67	54	7131	7348	7039	0	0	2				0					0	7
13	Future Park	406	68	0	3814	2912	2968	0	0	0				0					0	624
14	Commercial	1462	75	0	8382	8815	8535							0					0	0
15	North St.	848	78	0	11370	11816	11620							1					90	10
16	Commercial&Fulton	1152	83	0															0	0
17	Play Area	1680	92	0	4530	5369	5387							0						0
18	Mercantile Mall	1187	103	0	4921	5853	5942							0						0
19	New England T&T	1750	118	0	848	769	1043							0						
20	Marshall St.	102	122	0	0	94	67				218	182	172	127	71					
21	Hanover St. Bldg	163	123	36	0	139	161				31	50	17	31	0					
22	Parking Garage	634	123	0	0	2304	2835				0	0	0	0	0					
23	South Market St.	912	126	0										117						
24	Creek Square Bldg	506	132	74	0	50	30				0	0	0	0	0					
25	State St. Bldg	1203	153	0							0	0	0	1178	1					
26	Faneuil Flower Mkt.	691	155	0							0	0	0	901	2					
27	Hanover St. Bldg	173	157	55	0	30	9				1678	2422	2510	1483	27					
28	Congress St. Bldg	890	169	0							1	23	0	2313	12					
29	Congress St.	1421	172	0							18	12	2	3947	18					
30	Union St.	173	178	0							1247	1384	1251	964	114	2				
31	Boston City Hall	522	191	120							7708	7541	6068	3467	17	0				
32	Boston City Hall	915	199	0							1145	1392	815	2616	54	10				
33	Fed. Bldg. Plaza	326	227	0							1123	1561	1290							
34	Pool	832	230	0							723	631	481	44	3455	10				
35	New Fed. Bldg	301	236	0							725	1043	871	60	396	12	0			
36	JFK Fed. Bldg	816	248	355							0	0	0	0	2767	36	0	0		
37	New Fed. Bldg	314	254	69							6	3	9	0	1776	1019	0	19		
38	State Service Center	1376	289	0				0	0	0	0	0	0		0	124	2869	19	0	
39	Portland St.	810	297	0				0	0	0					0	0	333	527	0	
40	Market St.	704	310	0				0	0	0					0	0	0	2409	0	
41	Sudbury	282	315	0				239	96	265					5	67	230	851	24	
42	Canal & Causeway	1552	320	0				0	0	0						0	0	1485	0	
43	Canal St.	752	320	0				4	1	18						0	0	1440	0	0
44	Gov. Center Garage	352	321	107				1083	635	1344						0	0	2475	592	0
45	New Boston Gardens	1701	321	0												0	0	1471	0	0
46	New Boston Gardens	1701	321	400												0	0	2508	0	0
47	Vent Bldg-Upper	224	334	75				1046	755	630						2	5	885	289	11
48	Vent Bldg-Bottom	224	335	0				798	200	147						80	85	645	88	24
49	Washington	1069	344	0				1937	948	915						0	0	161	721	2

note $K^{\wedge} = (\chi U/Q)*10^{9}$ $[ft^{-2}]$

Table 17 Concentration Results (continued)

Run no. =				33	34	35	36	37	38	39	40	41	42	43	44	45	46	47	48
Point No.	Description	X (ft)	Y (Deg)	Z (ft)	K^	K^	K^	K^	K^	K^	K^	K^	K^	K^	K^	K^	K^	K^	K^	K^
1	N 600m Downwind	1968	0	0	0	0									0	0	1	5	0	0
2	St. Mary's School	765	8	0	23	0									0	0	0	0	0	3
3	Basketball Court	602	22	0	830	51									0	0	0	0	0	4
4	C.C. Youth Center	1078	33	19	2361	11									0	0	0			
5	Existing Road	342	36	55	2554	21	0							2421	1539	29				
6	NE 600m Downwind	1968	45	0	1988	11								0	16	5				
7	Prince St.	1219	46	0	3867	20	0							525	915	100				
8	Hanover St.	899	48	0	3666	45	0							1978	2508	168				
9	Blackstone St.	102	53	0	625	131	217	93						3641	1378	84				
10	Boston Police Acad.	749	62	0	1880	333	12	5						9755	7903	1487				
11	ENE 600m Downwind	1968	67	0	1080	5	0	0						2027	2501	1200				
12	Callahan Tunnel Bldg	1165	67	54	1265	227	0	0						5766	6191	2124				
13	Future Park	406	68	0	3027	261	0	0						9228	6675	458				
14	Commercial	1462	75	0	440	2478	2	0						7898	6783	2745				
15	North St.	848	78	0	1080	1274	0	0						14181	10887	2495				
16	Commercial&Fulton	1152	83	0		3606	71									2766				
17	Play Area	1680	92	0	41	4027	226	0						5854	3975	1208				
18	Mercantile Mall	1187	103	0	56	2737	1068	1						8188	5194	1157				
19	New England T&T	1750	118	0	0	96	702	1						2559	1685	327				
20	Marshall St.	102	122	0	81	49	51	204						210	102	28				
21	Hanover St. Bldg	163	123	36		40	16	495	0	0	0	0	0	0	513	121	13			
22	Parking Garage	634	123	0		150	541	14	0	0	0	0	0	0	4570	2684	335			
23	South Market St.	912	126	0	3	0	0	724	0	0	0				292	189	29			
24	Creek Square Bldg	506	132	74		2	113	417	0	0	0	0	3	0	21	26				
25	State St. Bldg	1203	153	0		0	0	1946	0	0	25	0	0	0						
26	Faneuil Flower Mkt.	691	155	0		0	0	838	0	0	0	0	0	0						
27	Hanover St. Bldg	173	157	55		14	12	964	191	415	104	0	0	0	23	24				
28	Congress St. Bldg	890	169	0			2	754	0	0	0	0	3	0						
29	Congress St.	1421	172	0			0	590	0	0	0	0	0	0						
30	Union St.	173	178	0			22	167	557	230	43	0	8	0						
31	Boston City Hall	522	191	120			0	0	5275	3099	263	4	0	0						
32	Boston City Hall	915	199	0				6	349	201	0	0	14	0						
33	Fed. Bldg. Plaza	326	227	0																
34	Pool	832	230	0				0	1460	390	23	778	871	550						
35	New Fed. Bldg	301	236	0				6	788	254	24	26	12	0						
36	JFK Fed. Bldg	816	248	355				0	0	5	0	2124	2093	3787				0	0	9
37	New Fed. Bldg	314	254	69				0	28	16	0	5734	1864	272				0	0	8
38	State Service Center	1376	289	0					0	0	0	0	0	0				4402	2466	548
39	Portland St.	810	297	0					0	0	0	0	0	0				13260	6817	884
40	Market St.	704	310	0					0	0	0	0	0	0				11296	4623	513
41	Sudbury	282	315	0					0	0	0	28	19	13				19340	5448	94
42	Canal & Causeway	1552	320	0								0	0	0				3083	1714	574
43	Canal St.	752	320	0								0	0	0			2	4240	1667	155
44	Gov. Center Garage	352	321	107								0	0	0			2	16010	5458	297
45	New Boston Gardens	1701	321	0								0	0	0			5	2193	1413	679
46	New Boston Gardens	1701	321	400													24	941	953	1656
47	Vent Bldg-Upper	224	334	75	0	32	25					0	5	110	0	0	2	7431	1755	330
48	Vent Bldg-Bottom	224	335	0	15							84	88	20	9	26		11203	3148	70
49	Washington	1069	344	0	0										0	0		29	0	5

note $K^{\wedge} = (\chi U/Q)*10^{9}$ $[ft^{-2}]$

Table 18 Concentration Results (continued)

Run no. =				49	50	51	52	53	54	55	56	61	62	63	64	65	66	67
Point No.	Description	X (ft)	Y (Deg)	Z (ft)	K^	K^	K^	K^	K^	K^	K^	K^	K^	K^	K^	K^	K^	K^	K^
1	N 600m Downwind	1968	0	0							2	0	0	0	0	0	4	22	0
2	St. Mary's School	765	8	0							0	0	24	0	0	1266	1	8	0
3	Basketball Court	602	22	0							0	0	29	0	0	1390	1	8	0
4	C.C. Youth Center	1078	33	19								2	0	0	0	58	0	19	1
5	Existing Road	342	36	55								164	452	111	0	274	0	8	0
6	NE 600m Downwind	1968	45	0								4	0	0	0	1	0	28	18
7	Prince St.	1219	46	0								352	0	0	0	4	0	18	1
8	Hanover St.	899	48	0								872	0	0	0	751	0	24	4
9	Blackstone St.	102	53	0	235	63						254	2465	660	64	14	43	24	3
10	Boston Police Acad.	749	62	0	43	5						3038	1	0	0	2392	8	30	9
11	ENE 600m Downwind	1968	67	0	16	1						1837	11	0	0	0	0	2	0
12	Callahan Tunnel Bldg	1165	67	54	1	0						3663	0	0	0	342	0	16	0
13	Future Park	406	68	0	9	0						1122	297	75	0	538	0	13	0
14	Commercial	1462	75	0	171	0						3145	5	0	0	99	0	2	0
15	North St.	848	78	0	38	1						3094	11	0	0	1997	6	13	0
16	Commercial&Fulton	1152	83	0								3140	19	3	1	2083	11	8	0
17	Play Area	1680	92	0	0	1						1603	0	0	0	661	0	3	0
18	Mercantile Mall	1187	103	0	169	10						1494	4	0	0	1930	3	4	0
19	New England T&T	1750	118	0	3316	775		0				455	34	0	0	1124	0	8	0
20	Marshall St.	102	122	0	646	147		40	0	0		29	2543	723	69	21	35	29	4
21	Hanover St. Bldg	163	123	36	2151	706		0	0	0		56	2452	690	74	9	27	36	0
22	Parking Garage	634	123	0	6803	1284		0	0	0		455	969	333	37	63	0	8	0
23	South Market St.	912	126	0	1684	1088		0	0	0		68	1958	934	222	11	1	5	0
24	Creek Square Bldg	506	132	74	6275	2256		0	0	0			2022	784	103	7	2	9	0
25	State St. Bldg	1203	153	0	0	20		0	0	0			4040	2423	931	14	5	4	0
26	Faneuil Flower Mkt.	691	155	0	75	56		0	0	0			3686	1686	524	13	12	8	0
27	Hanover St. Bldg	173	157	55	340	171		1074	0	0			3237	1035	183	13	22	19	3
28	Congress St. Bldg	890	169	0	0	7	0	0	0	0			3382	1821	635	11	13	14	5
29	Congress St.	1421	172	0	0	3	0	0	0	0			2973	1713	813	11	16	8	0
30	Union St.	173	178	0	50	30	0	145	0	0			3026	1124	260	11	56	43	11
31	Boston City Hall	522	191	120	0	2	0	1066	16	0			2933	1359	445	10	103	11	0
32	Boston City Hall	915	199	0	5	3	0	21	9	0			587	107	86	1	231	36	28
33	Fed. Bldg. Plaza	326	227	0															
34	Pool	832	230	0	0	1	762	324	140	572	0		459	99	54	0	2107	79	8
35	New Fed. Bldg	301	236	0	0	5	0	146	0	0			1943	712	153	6	275	55	69
36	JFK Fed. Bldg	816	248	355			2972	1	15	3460	0		38	3	3	0	4269	88	7
37	New Fed. Bldg	314	254	69	0	1	802	0	0	351	0		1860	690	185	6	568	81	14
38	State Service Center	1376	289	0			7		0	16	1222		0	0	0	0	619	5883	751
39	Portland St.	810	297	0			24		0	13	1904		508	47	5	0	1050	651	46
40	Market St.	704	310	0			11		0	6	1047		1158	315	18	1	493	1123	174
41	Sudbury	282	315	0						0	13		2447	544	26	9	183	69	96
42	Canal & Causeway	1552	320	0						5	889		8	0	0	0	18	1552	7921
43	Canal St.	752	320	0						2	240	0	646	126	0	4	495	1363	405
44	Gov. Center Garage	352	321	107						0	246	0	4366	1414	119	22	40	14	2
45	New Boston Gardens	1701	321	0						3	810	1	1[illegible]	0	0	0	21	1443	13681
46	New Boston Gardens	1701	321	400							1196	14	0	0	0	6	0	2030	12422
47	Vent Bldg-Upper	224	334	75							13		2447	726	47	14	51	36	6
48	Vent Bldg-Bottom	224	335	0							0		471	92	11	14	147	211	185
49	Washington	1069	344	0							0		61	0	0	110	3	20	100

note $K^{\wedge} = (\chi U/Q)*10^{9}$ $[ft^{-2}]$

Table 19 Concentration Results for Runs 57, 58, 59 and 60

RUN NO. =			57	58	59	60
X (ft)	Y (ft)	Z (ft)	K^	K^	K^	K^
256	-384	0	3	0	0	0
256	-256	0	13	134	0	0
256	-129	0	159	3483	49	0
256	0	0	1803	5148	912	496
256	129	0	245	3575	131	2382
256	256	0	6	20	167	225
256	384	0	3	2	3	0
960	-640	0	3	0	0	0
960	-480	0	3	0	0	0
960	-320	0	138	170	3	0
960	-160	0	1800	3122	552	382
960	0	0	3301	8600	4053	2707
960	160	0	1258	3493	3351	3209
960	320	0	56	512	370	414
960	480	0	3	2	3	0
960	640	0	0	0	0	0
1664	-769	0	3	0	0	0
1664	-576	0	3	0	0	0
1664	-384	0	145	195	63	36
1664	-192	0	1825	3233	1033	1088
1664	0	0	3743	7441	4745	3983
1664	192	0	1465	3721	3076	2610
1664	384	0	95	623	488	542
1664	576	0	3	6	3	0
1664	769	0	0	0	0	0
2369	-896	0	38	38	6	0
2369	-672	0	38	38	6	0
2369	-449	0	181	255	117	136
2369	-224	0	933	1439	734	752
2369	0	0	1269	1974	1443	1284
2369	224	0	630	1404	922	859
2369	449	0	45	152	88	89
2369	672	0	10	13	3	0
2369	896	0	13	13	3	0

note K^ = (χU/Q) * 10^9 [ft^{-2}]

FIGURES

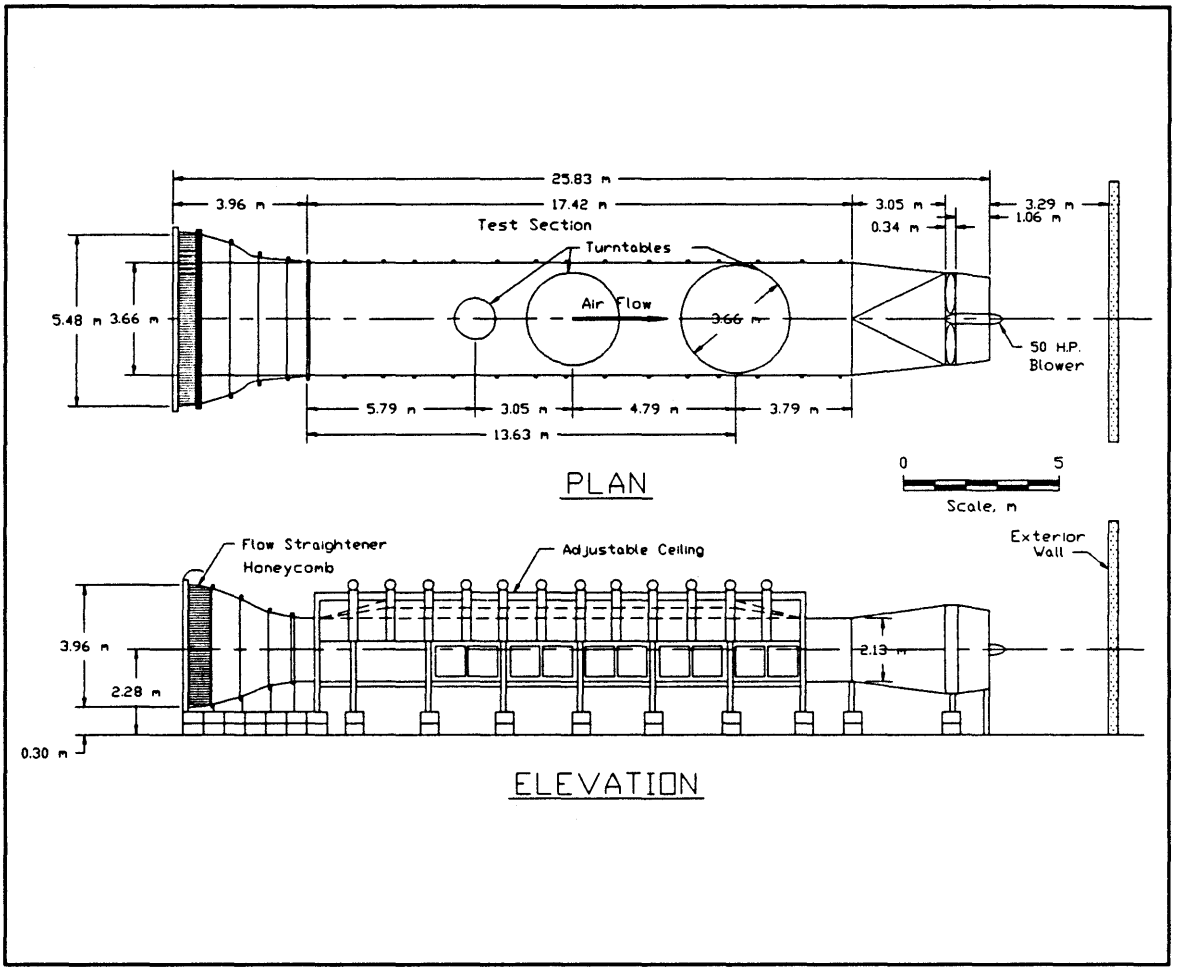

Figure 1 Environmental Wind Tunnel

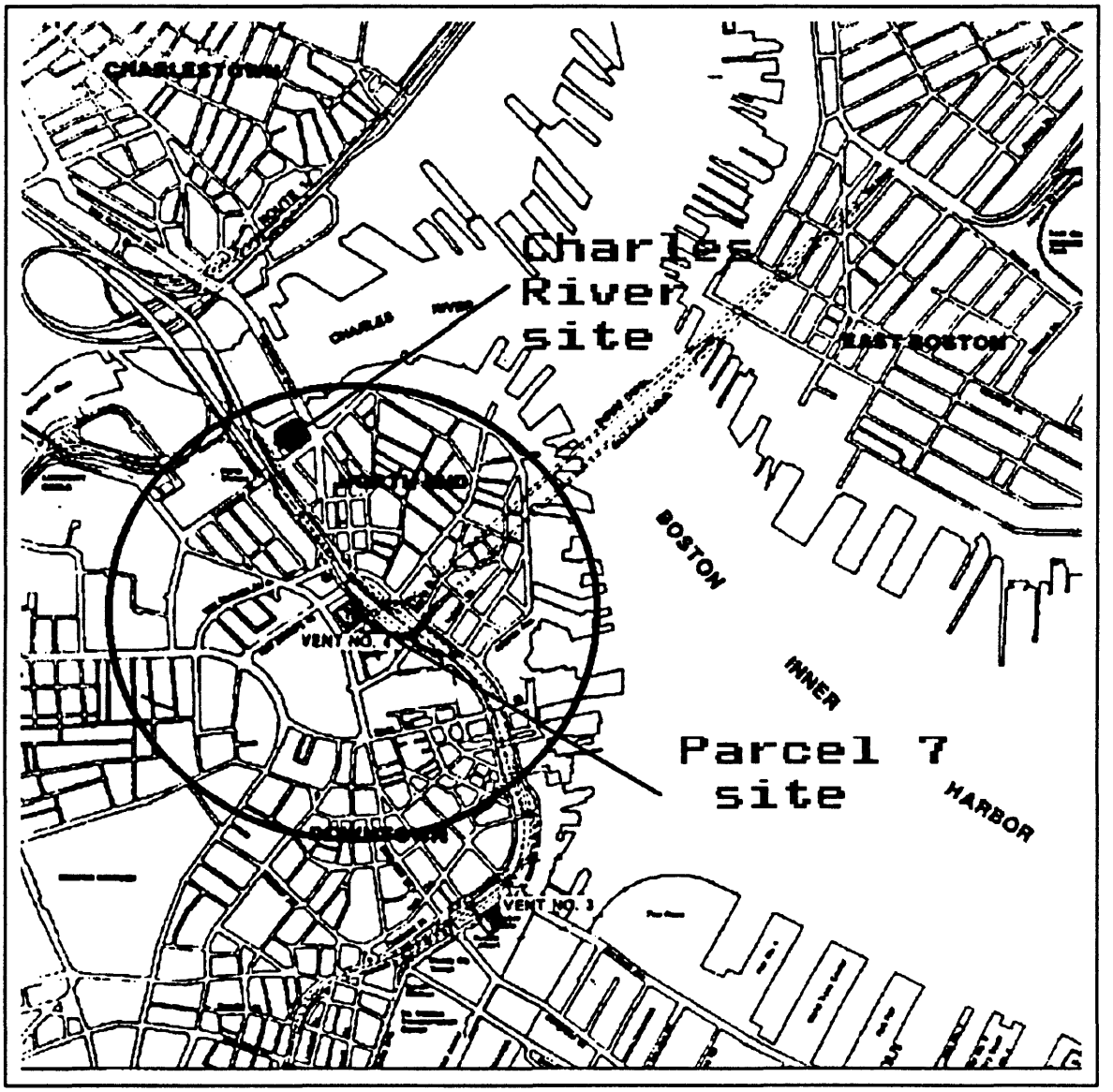

Figure 2 Parcel 7 model site on a map of Boston

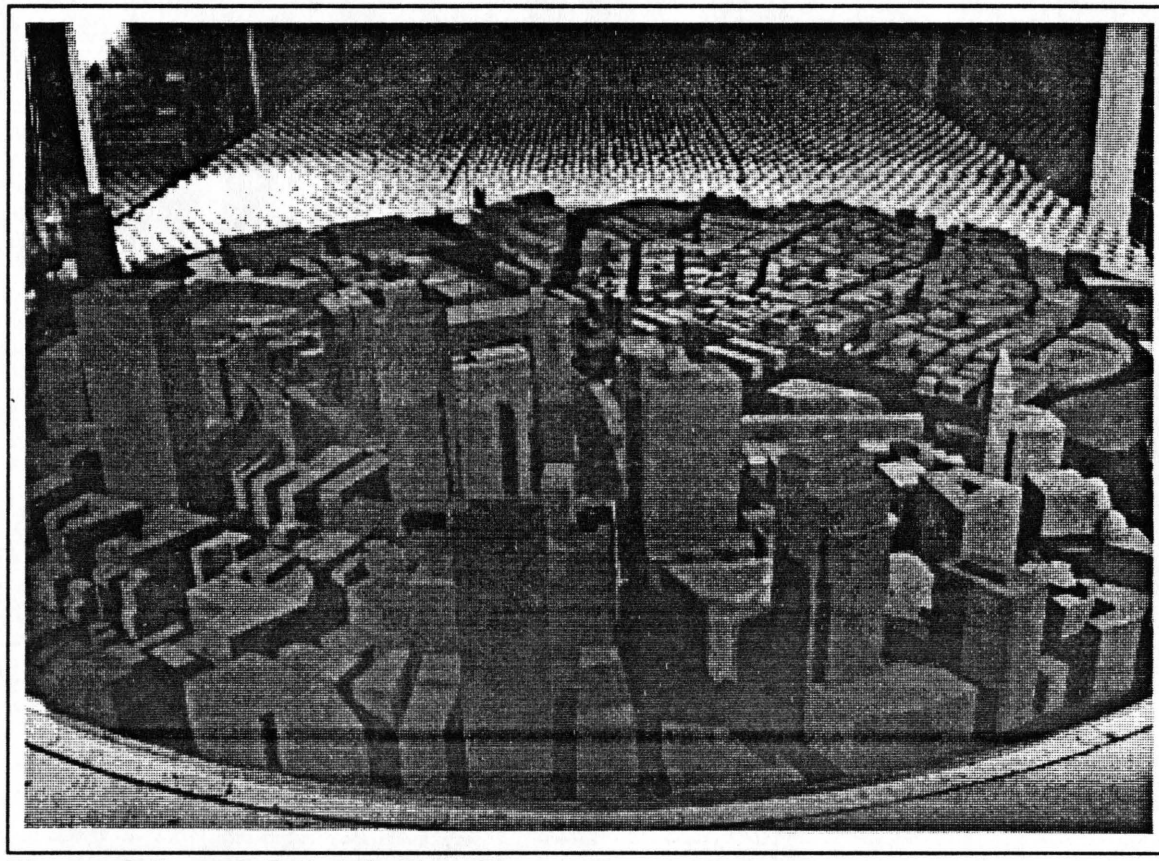

Figure 3 Parcel 7 Model Site Picture

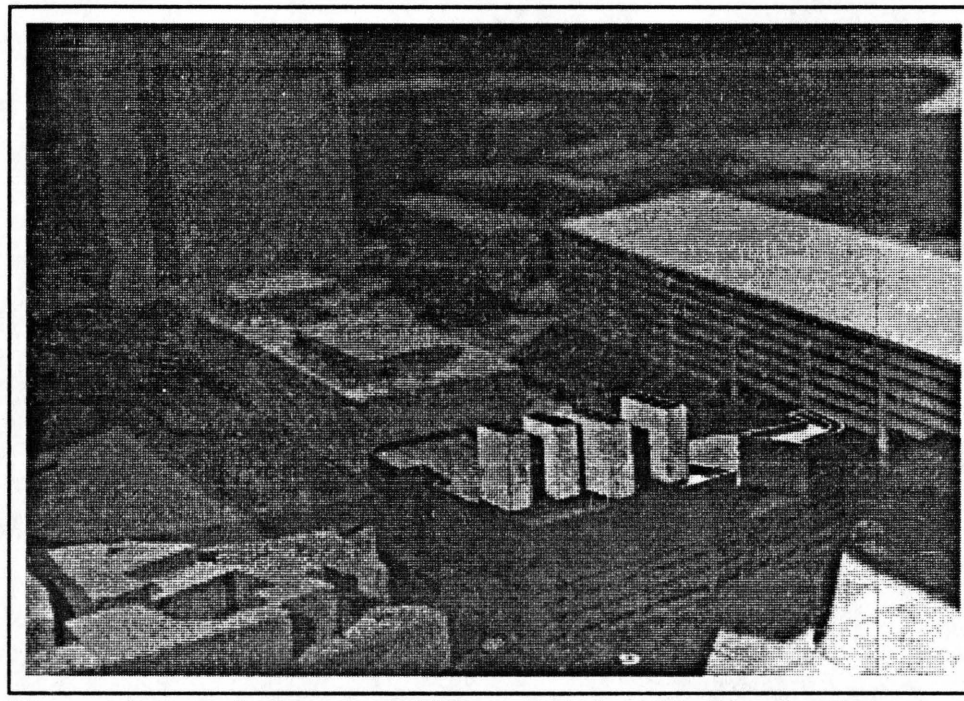

Figure 4 Parcel 7 Vent Building Model : 75 foot building and garage, 125 foot stacks (view 1)

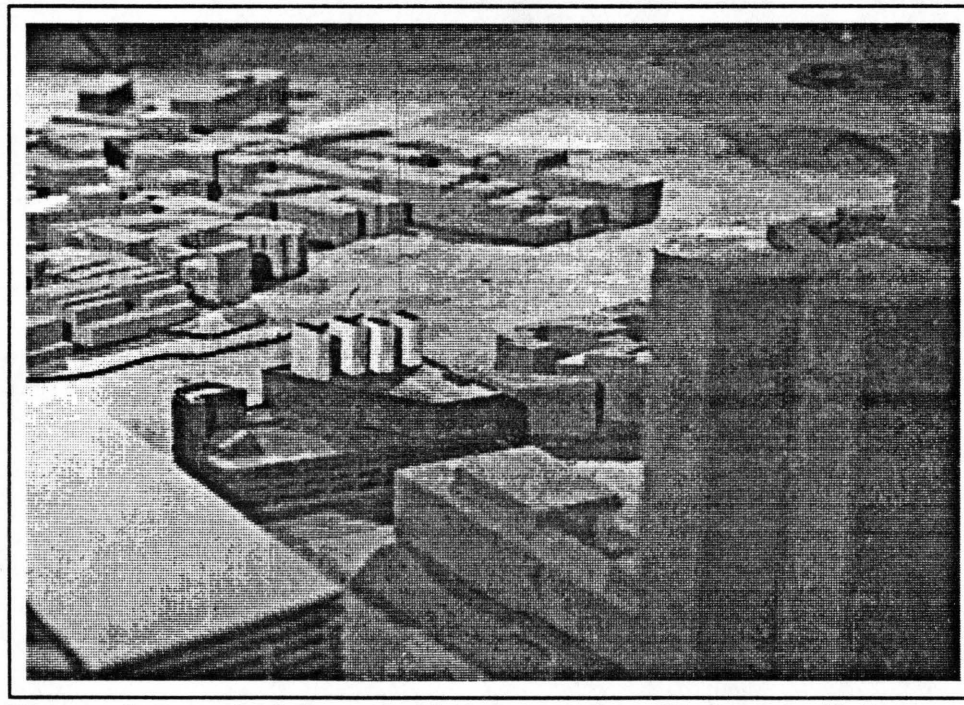

Figure 5 Parcel 7 Vent Building Model : 75 foot building and garage, 125 foot stacks (view 2)

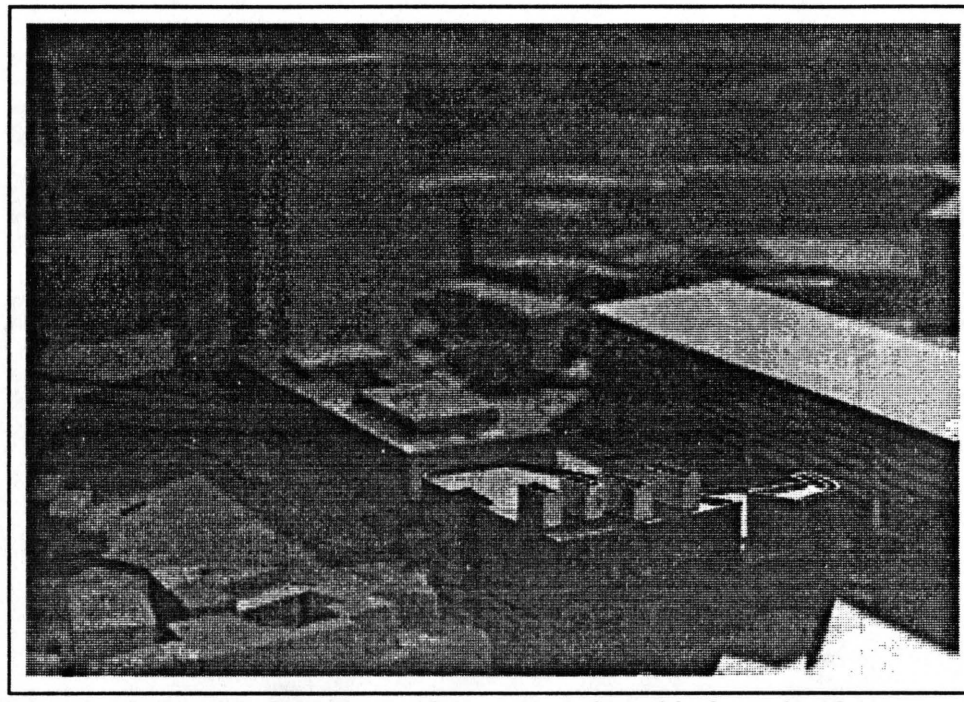

Figure 6 Parcel 7 Vent Building Model : 90 foot building and garage, 115 foot stacks

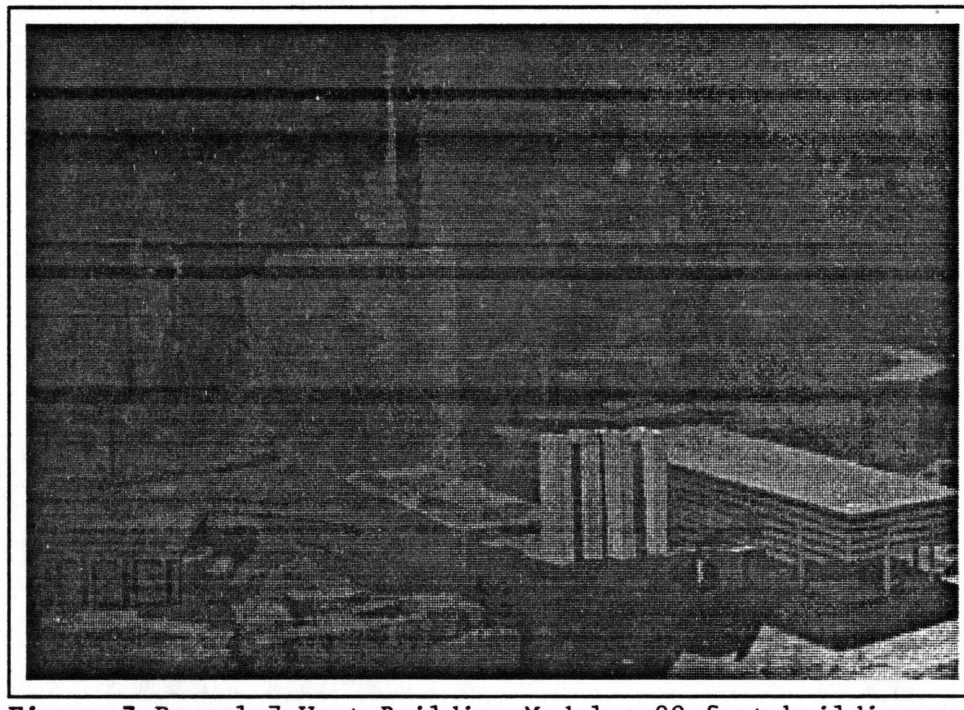

Figure 7 Parcel 7 Vent Building Model : 90 foot building and garage, 225 foot stacks

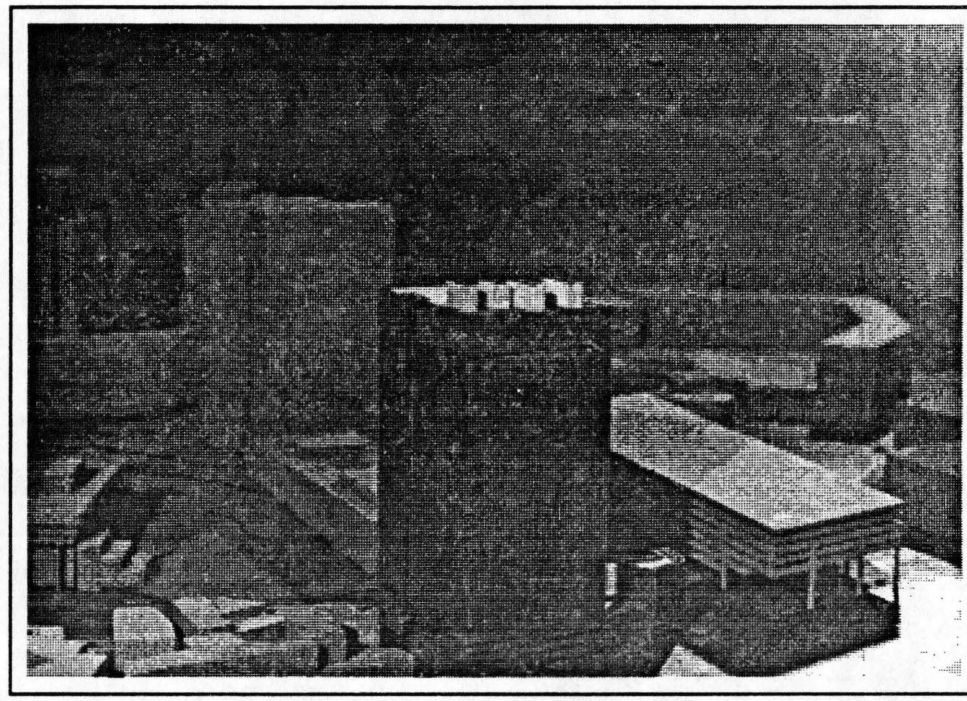

Figure 8 Parcel 7 Vent Building Model : 375 foot building, 42 foot garage and 400 foot stacks

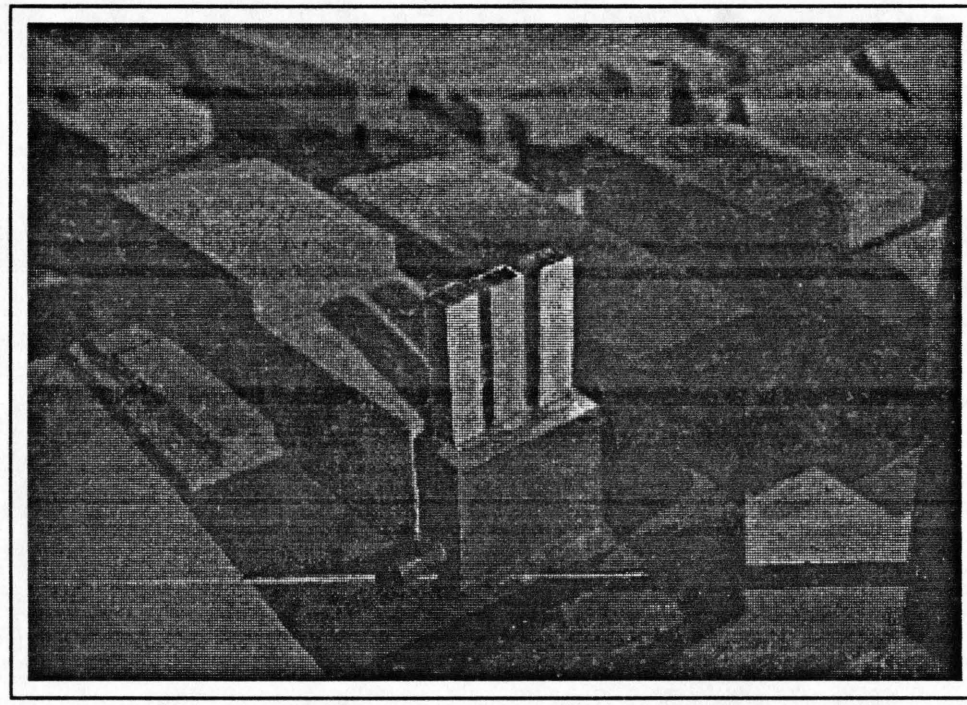

Figure 9 Charles river Vent Building Model : 100 foot building, 200 foot stacks

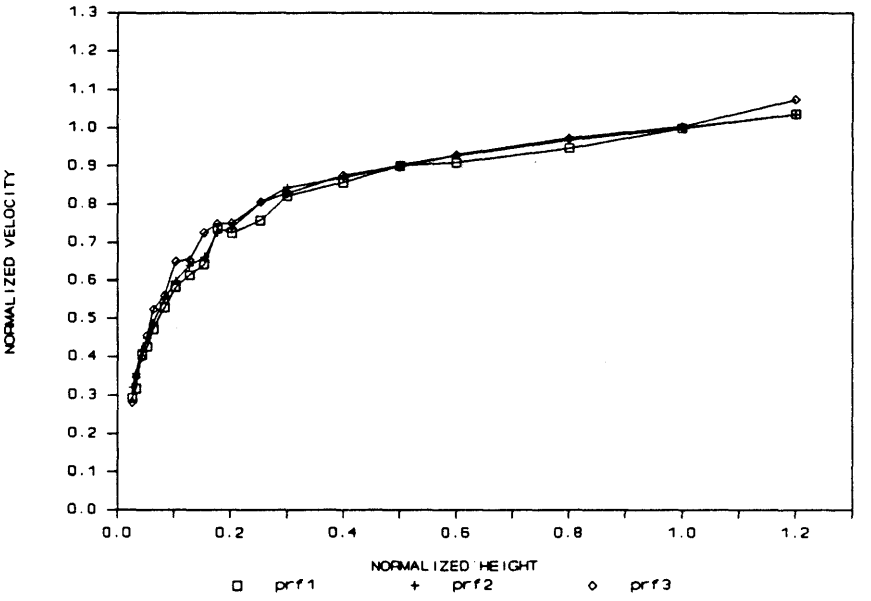

Figure 10 Mean Velocity Profiles for Profiles 1, 2 and 3

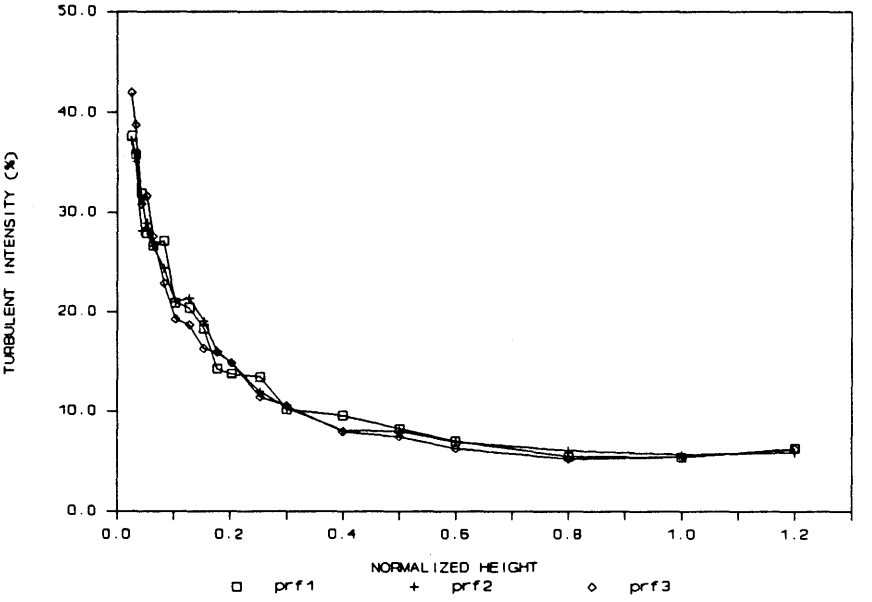

Figure 11 Turbulent Intensity Profiles for Profiles 1, 2 and 3

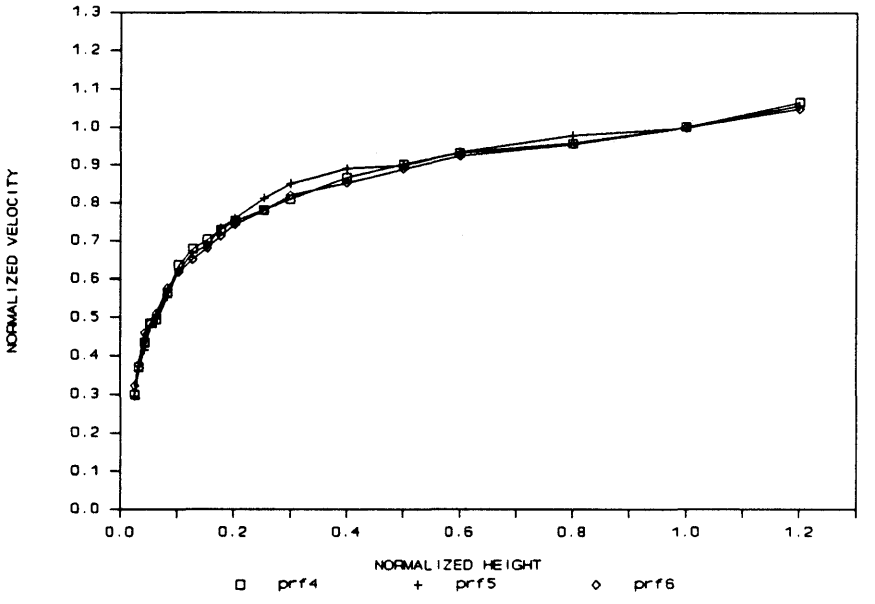

Figure 12 Mean Velocity Profiles for Profiles 4, 5 and 6

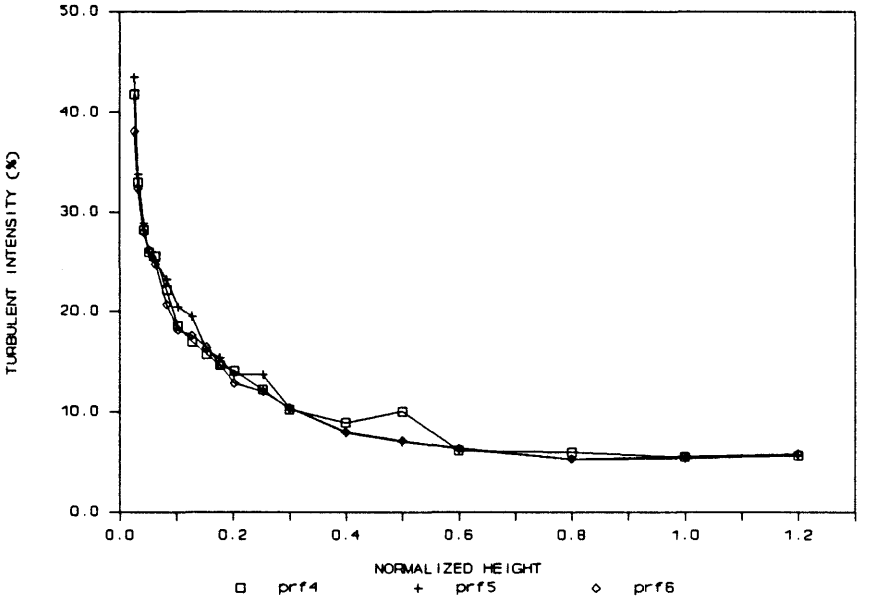

Figure 13 Turbulent Intensity Profiles for Profiles 4, 5 and 6

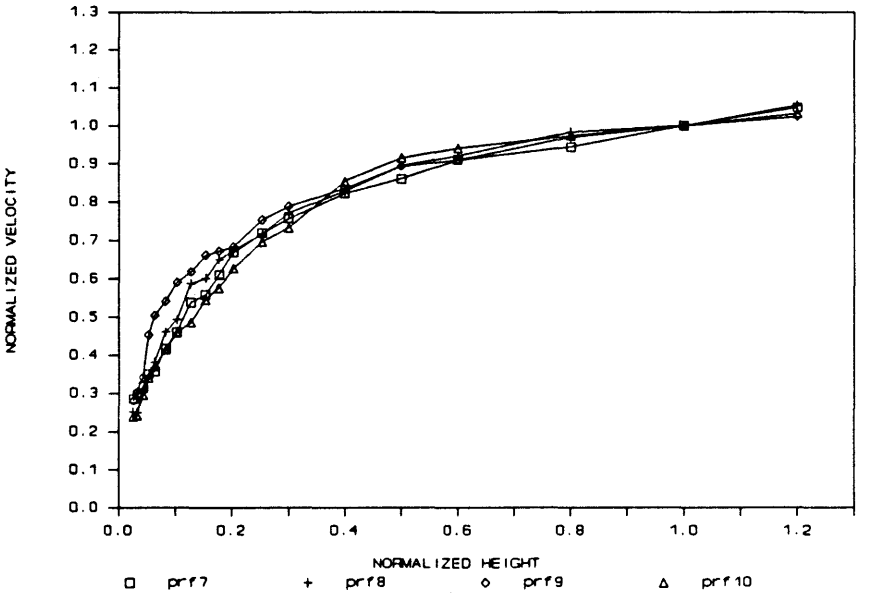

Figure 14 Mean Velocity Profiles for Profiles 7, 8, 9 and 10

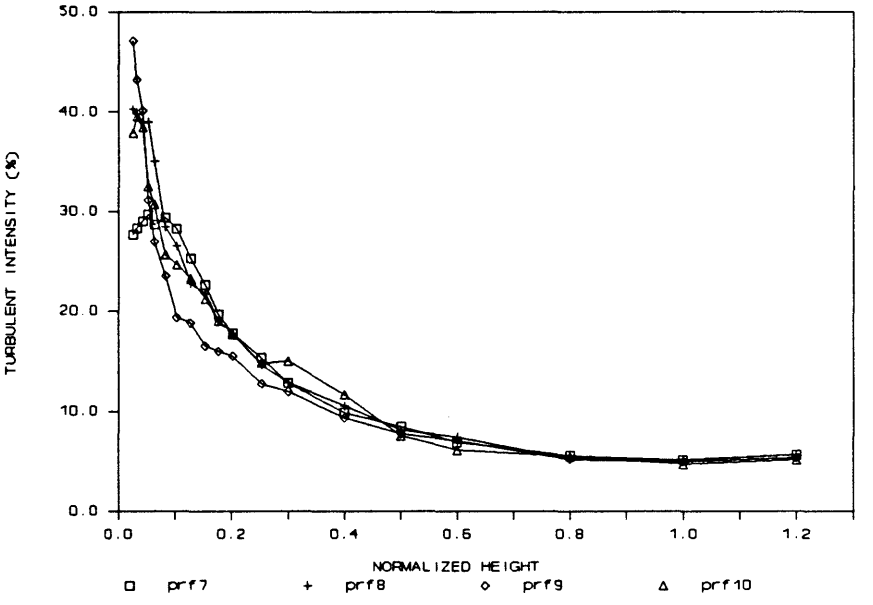

Figure 15 Turbulent Intensity Profiles for Profiles 7, 8, 9 and 10

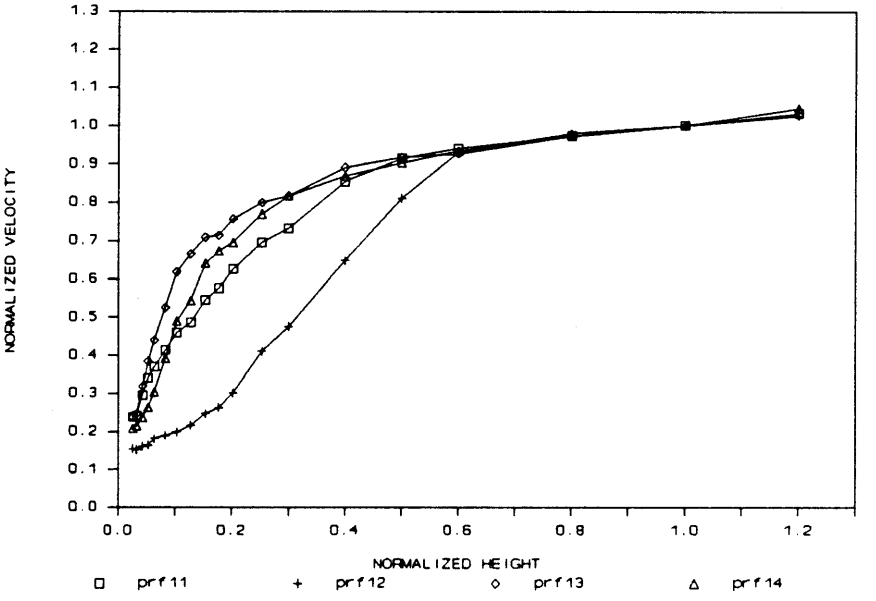

Figure 16 Mean Velocity Profiles for Profiles 11, 12, 13 and 14

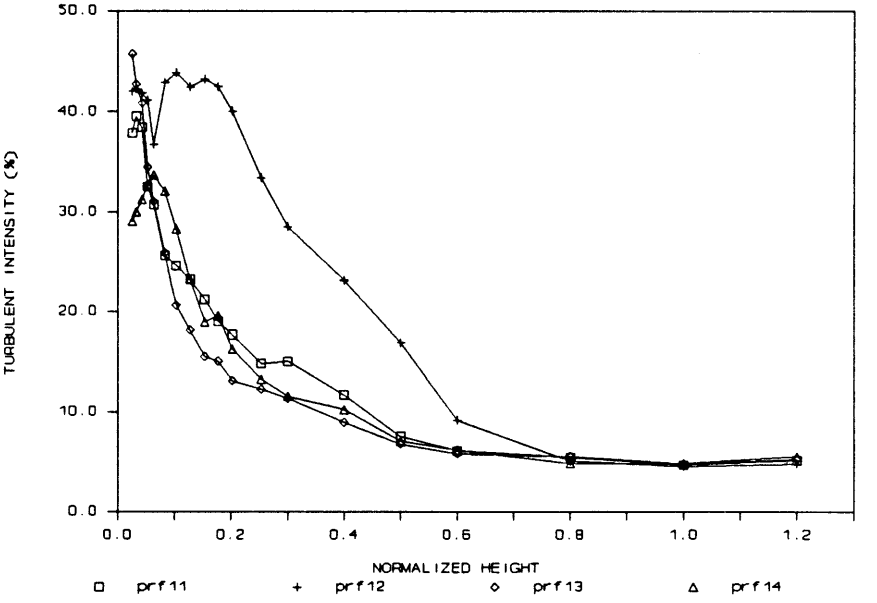

Figure 17 Turbulent Intensity Profiles for Profiles 11, 12, 13 and 14

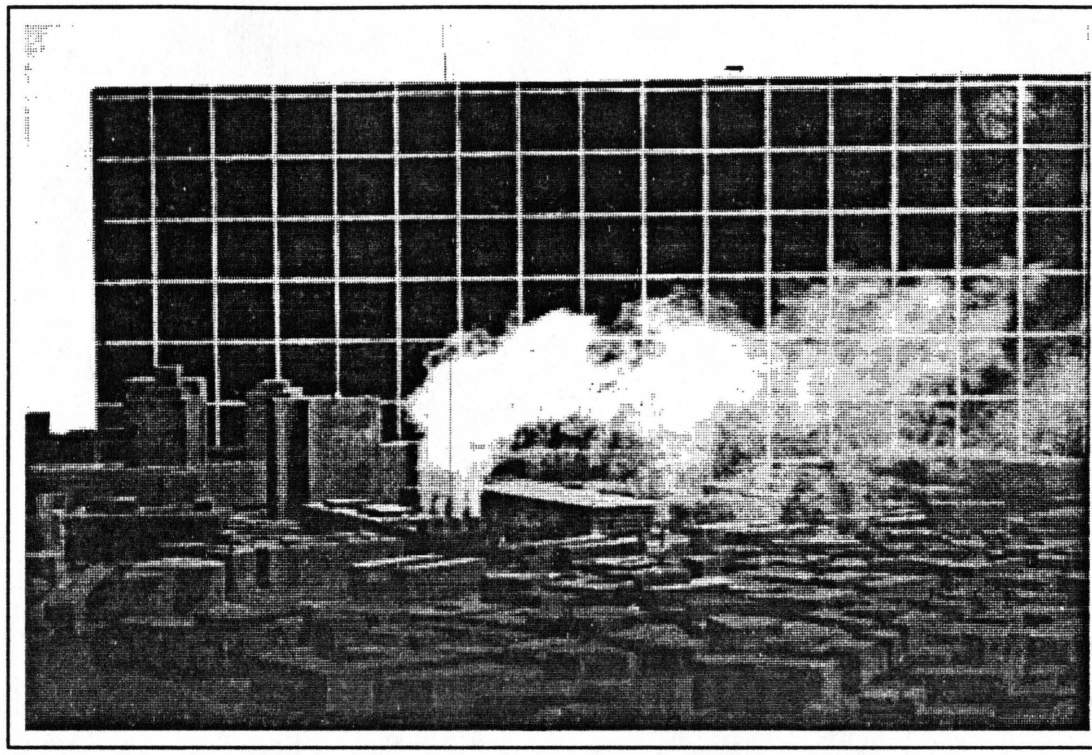

Figure 18 Plume Visualization from Parcel 7 Vent Site, Short Stacks

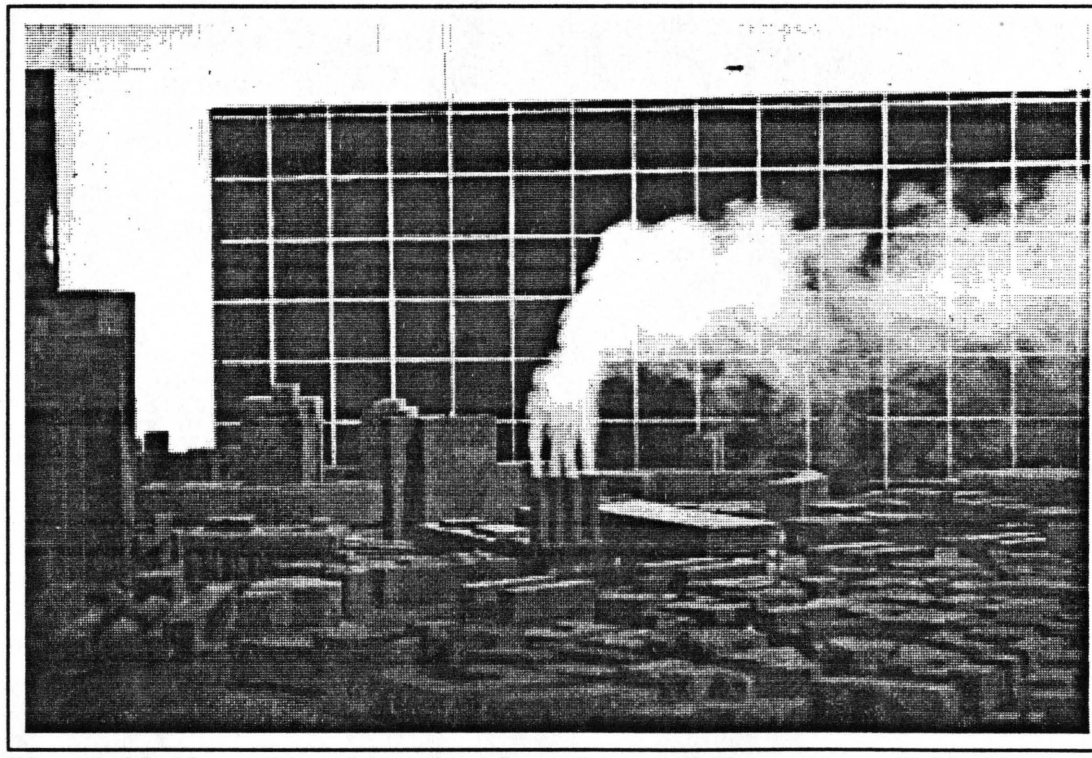

Figure 19 Plume Visualization from Parcel 7 Vent Site, Tall Stacks

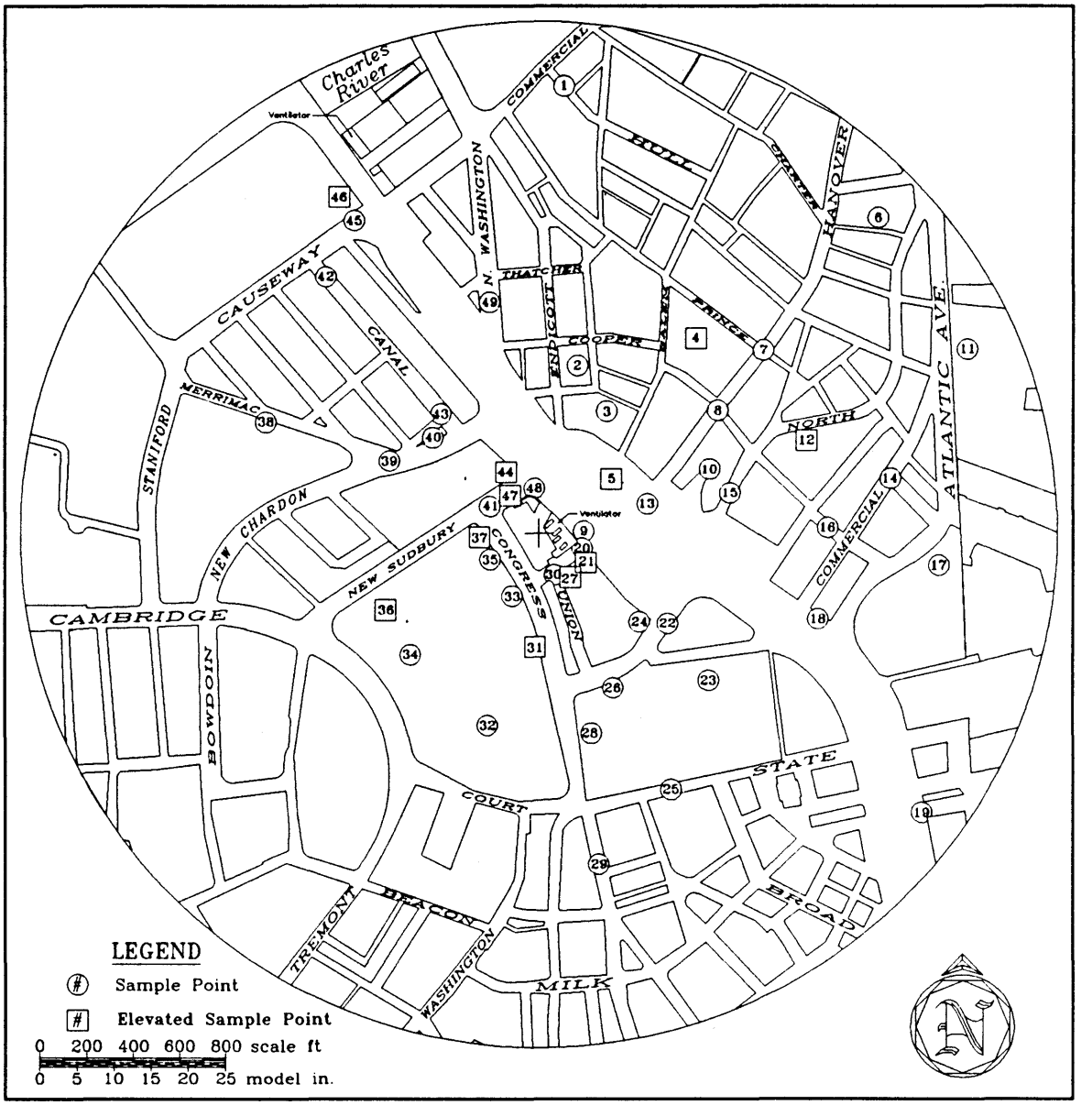

Figure 20 Concentration Sample Locations on a Site Map of the City of Boston

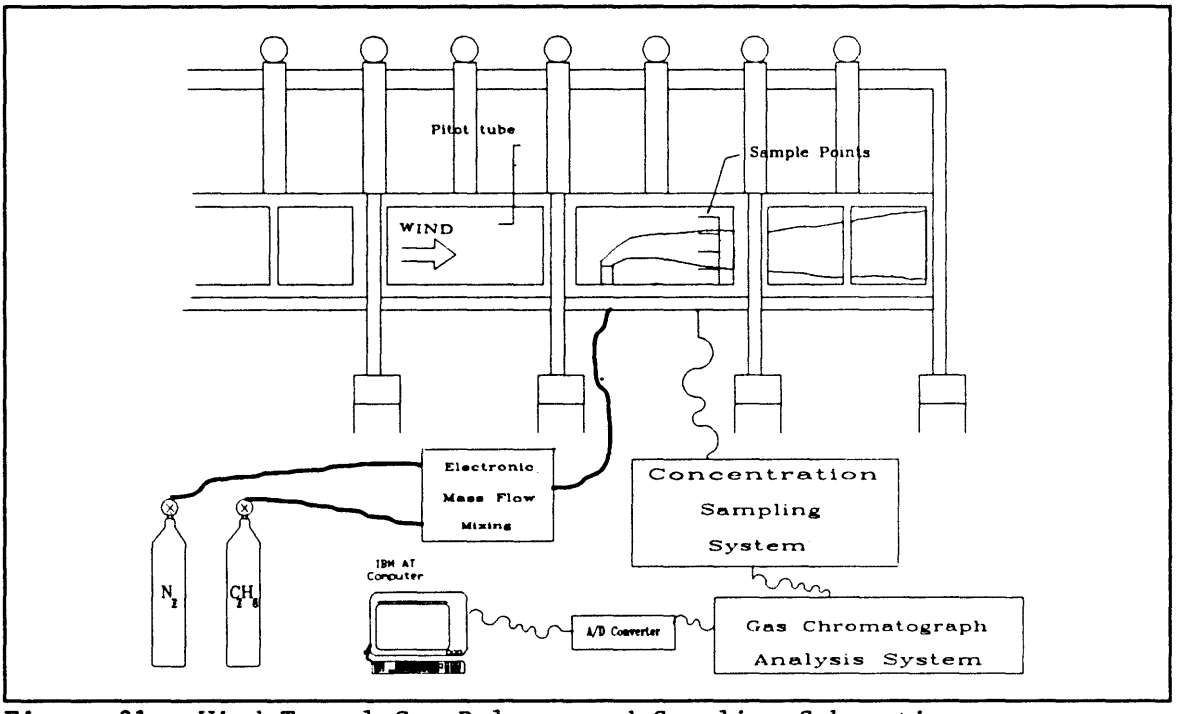

Figure 21 Wind Tunnel Gas Release and Sampling Schematic

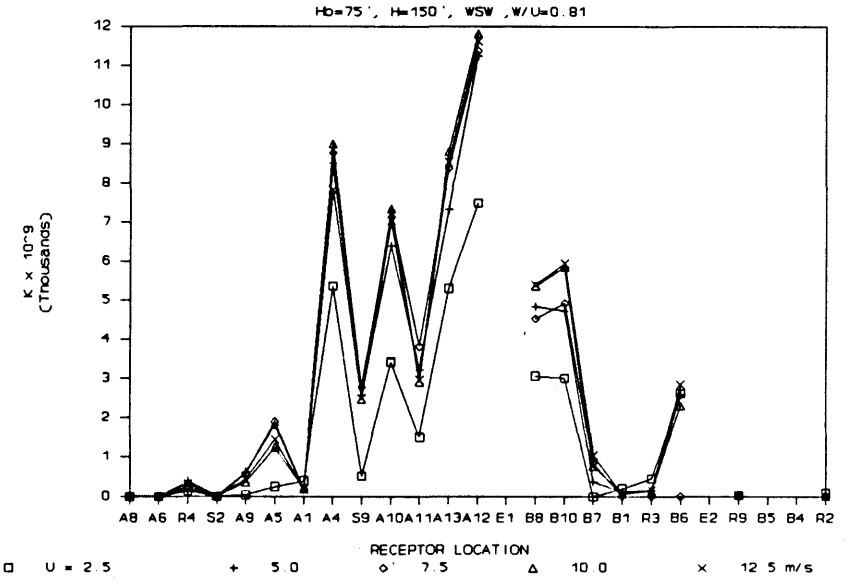

Figure 22 Reynolds number independence tests, Parcel 7, H_b = 75 ft, H = 150 ft, Wind direction WSW

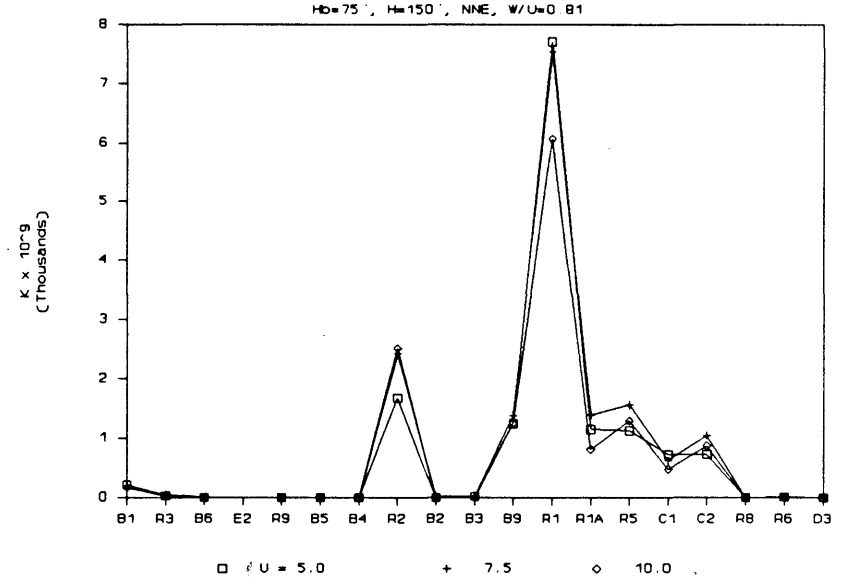

Figure 23 Reynolds number independence tests, Parcel 7, H_b = 75 ft, H = 150 ft, Wind direction NNE

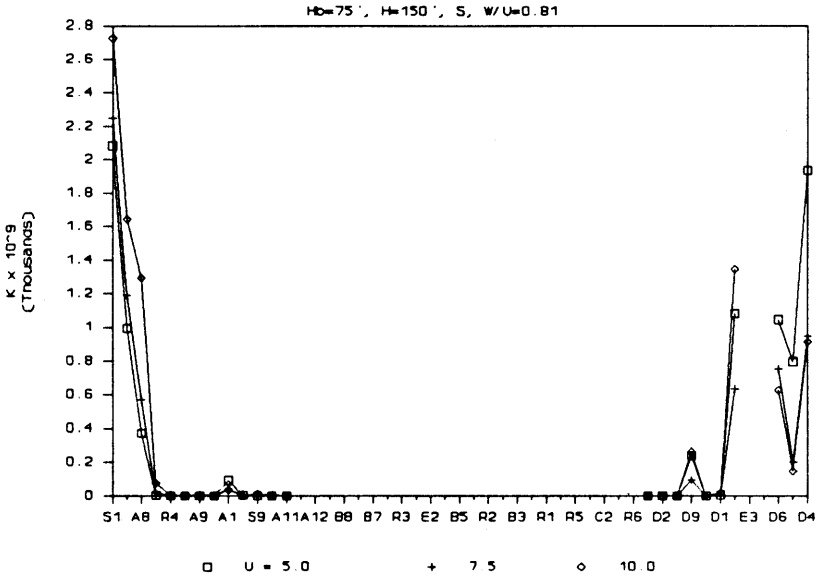

Figure 24 Reynolds number independence tests, Parcel 7, H_b = 75 ft, H = 150 ft, Wind direction S

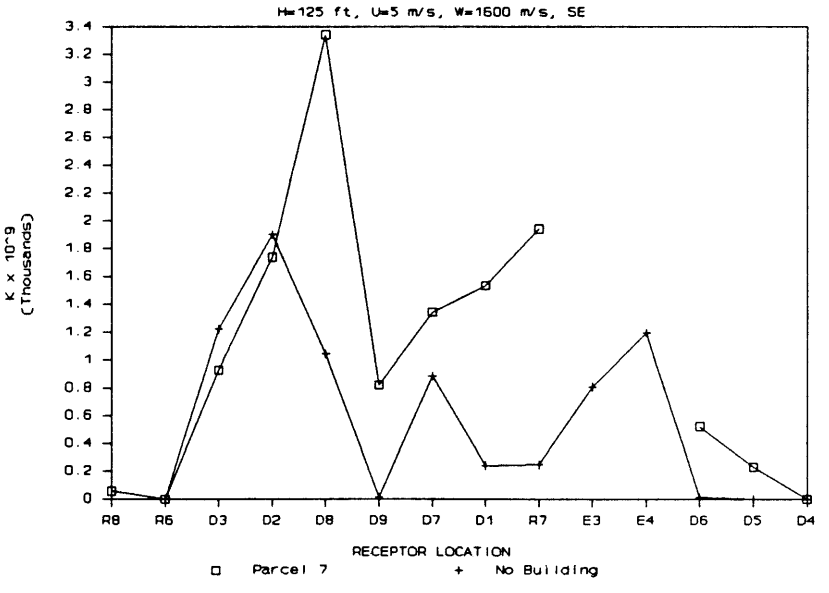

Figure 25 Building downwash effects through comparison between isolated 125 ft stack and ventilators on Parcel 7 Ventilation building.

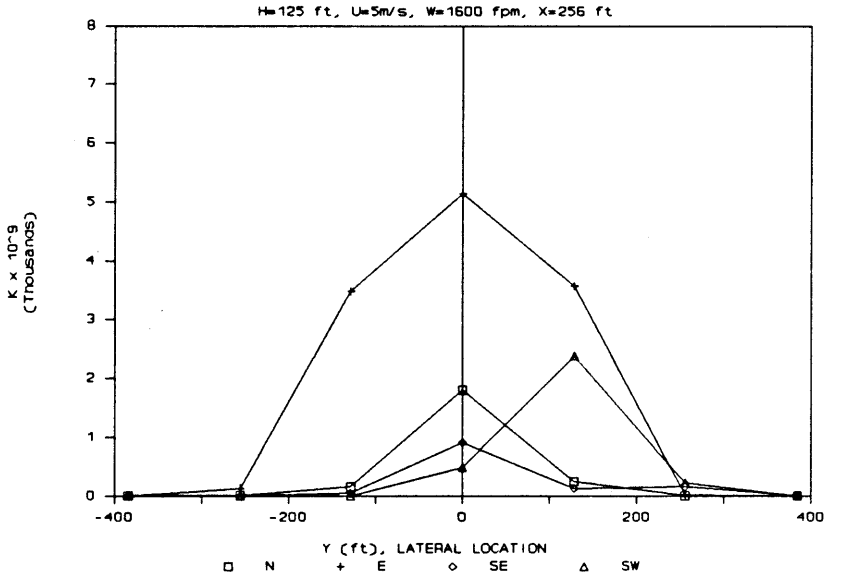

Figure 26 Groundlevel plume cross-sections downwind of Parcel 7 building, no city model present, X = 256 ft

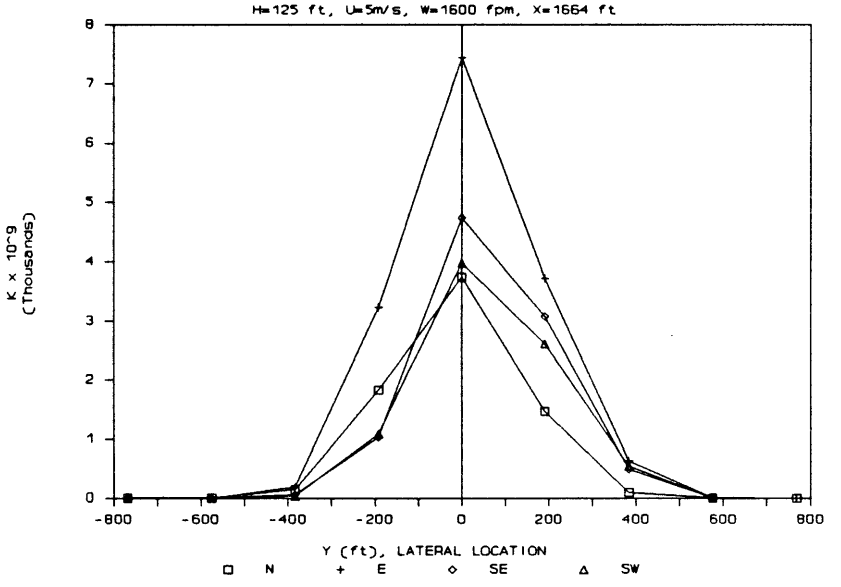

Figure 27 Groundlevel plume cross-sections downwind of Parcel 1 building, no city model present, X = 1664 ft

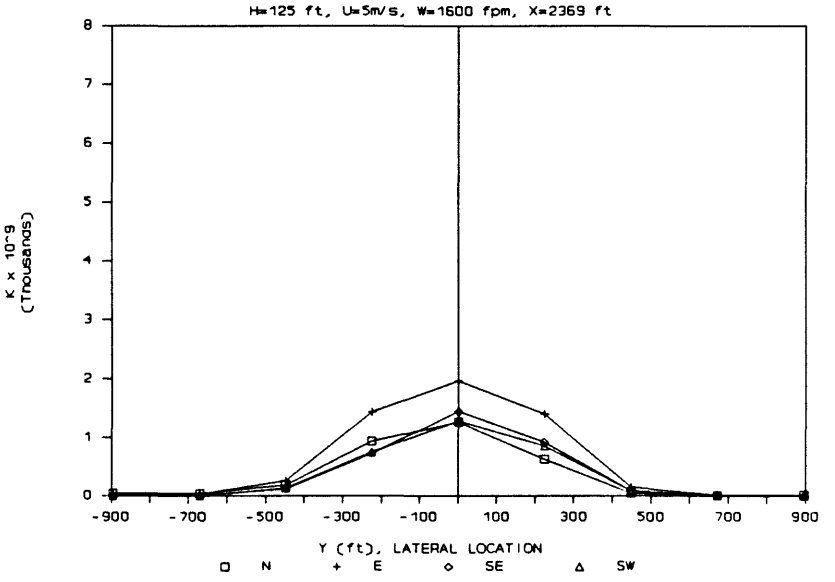

Figure 28 Groundlevel plume cross-sections downwind of Parcel 7 building, no city model present, X = 2369 ft

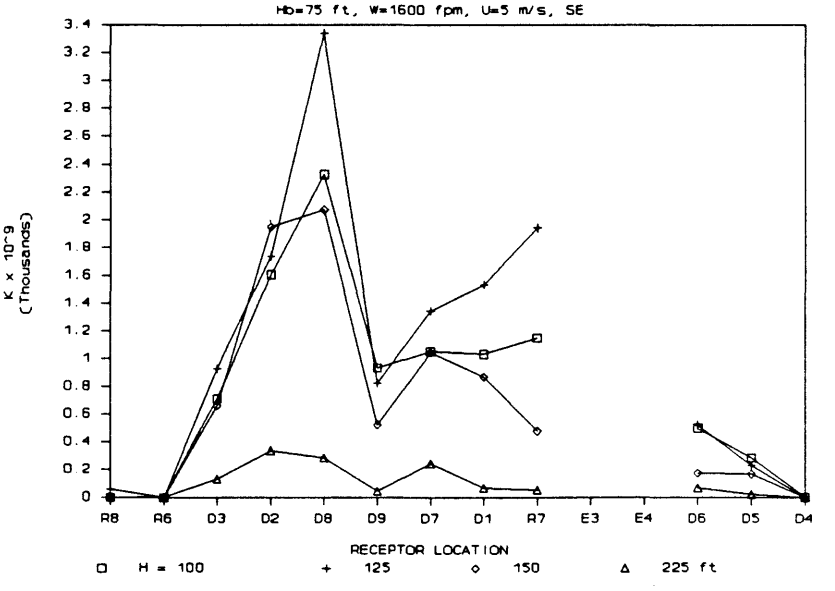

Figure 29 Influence of stack height on sampler concentrations, Wind direction SE

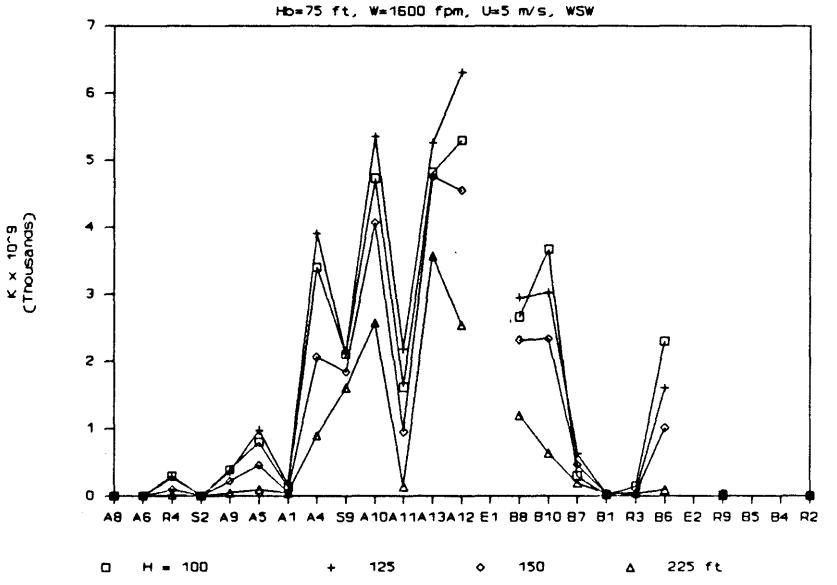

Figure 30 Influence of stack height on sampler concentrations, Wind direction WSW

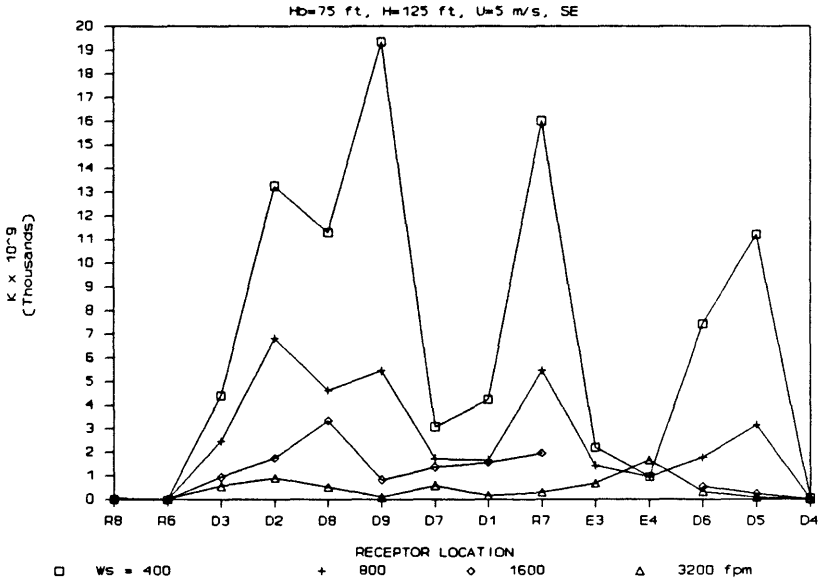

Figure 31 Influence of stack exhaust velocity on sampler concentrations

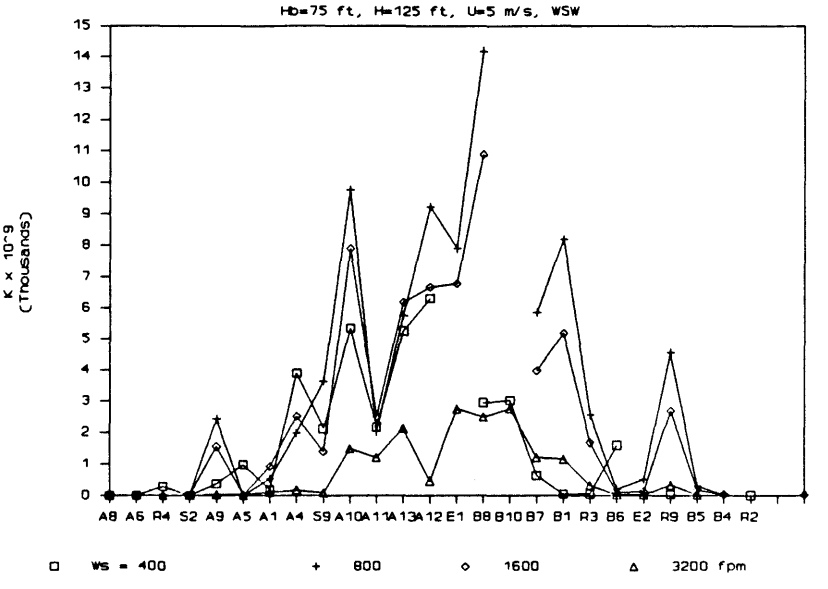

Figure 32 Influence of stack exhaust velocity on sampler concentrations, Wind direction WSW

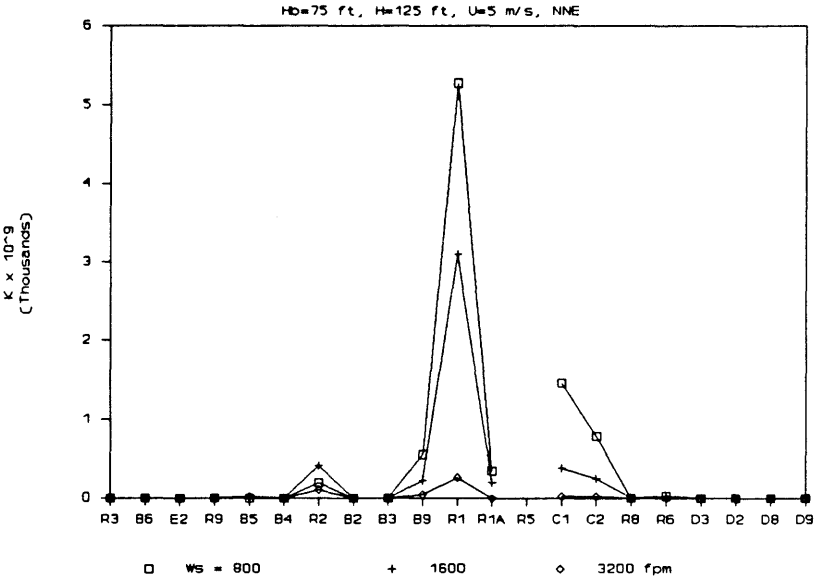

Figure 33 Influence of stack exhaust velocity on sampler concentrations, Wind direction NNE

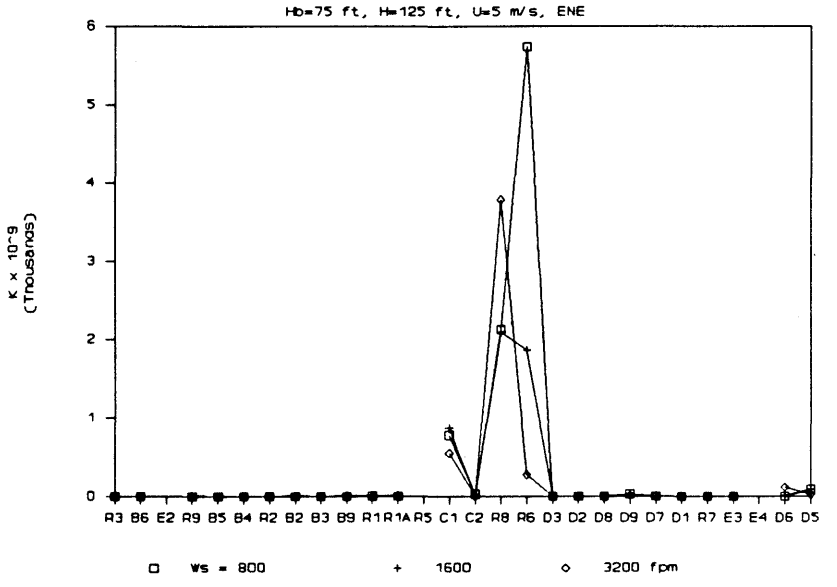

Figure 34 Influence of stack exhaust velocity on sampler concentrations, Wind direction ENE

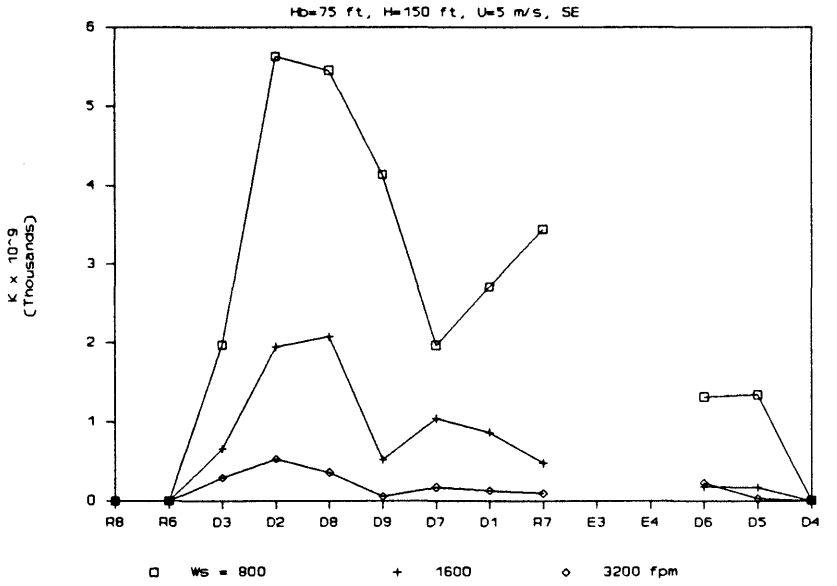

Figure 35 Influence of stack exhaust velocity on sampler concentrations, Wind direction SE

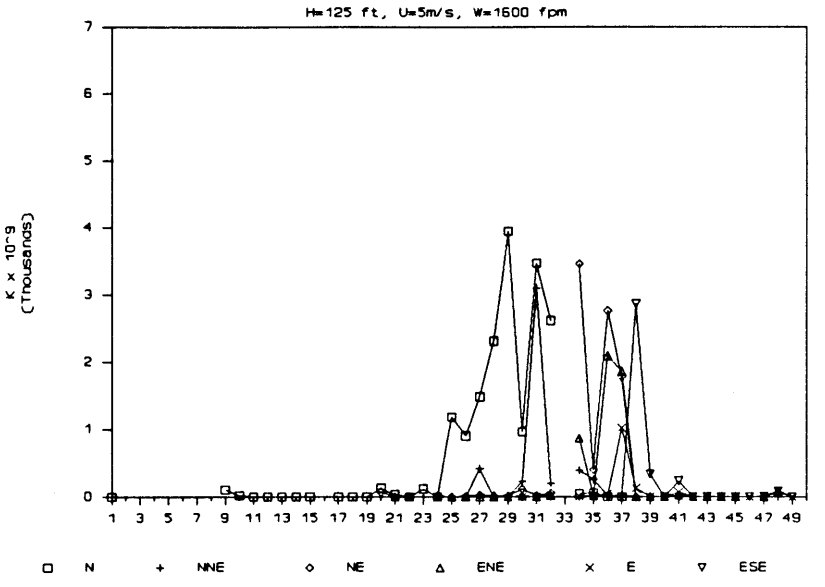

Figure 36 Influence of wind direction on sampler concentrations, N through ESE

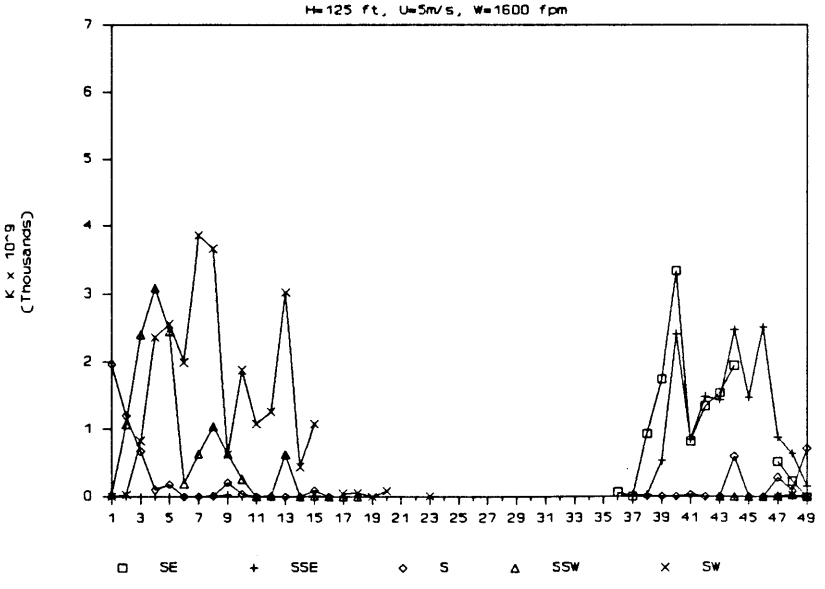

Figure 37 Influence of wind direction on sampler concentrations, SE through SW

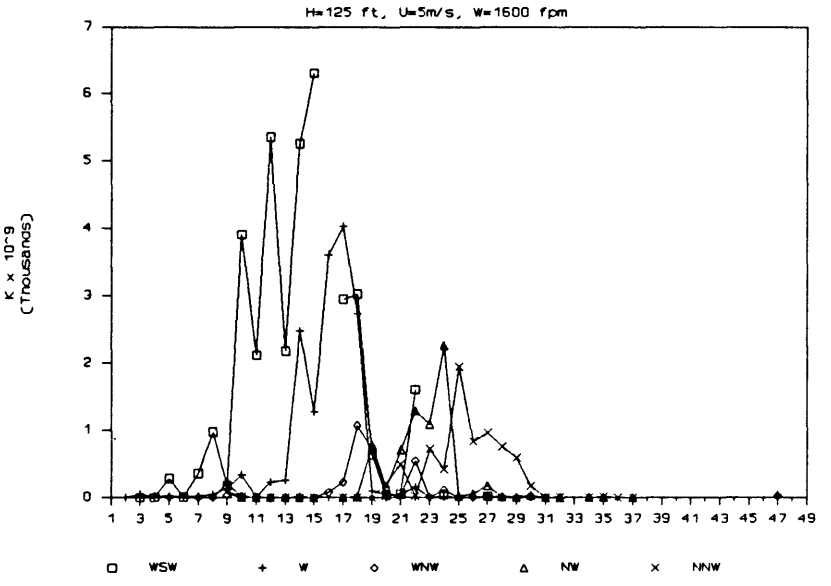

Figure 38 Influence of wind direction on sampler concentrations, WSW through NNW